UNIVERSITY OF ILLINOIS
URBANA

AERONOMY REPORT NO. 105

A ROCKET-BORNE ELECTRIC FIELD METER FOR THE MIDDLE ATMOSPHERE

by
G. J. Dettro
L. G. Smith

December 1, 1982

Library of Congress ISSN 0568-0581

Aeronomy Laboratory
Department of Electrical Engineering
University of Illinois
Urbana, Illinois

Supported by
National Aeronautics and Space Administration

UILU-ENG-82-2505

A E R O N O M Y R E P O R T

N O. 105

A ROCKET-BORNE ELECTRIC FIELD METER FOR THE MIDDLE ATMOSPHERE

by

G. J. Dettro
L. G. Smith

December 1, 1982

Supported by
National Aeronautics and
Space Administration
Grant NGR 14-005-181

Aeronomy Laboratory
Department of Electrical Engineering
University of Illinois
Urbana, Illinois

ABSTRACT

This paper presents the design and construction of a rocket-borne electric field meter to measure the atmosphere's electric field and conductivity in the middle atmosphere. The operating characteristics of the instrument are discussed and a proposed flight configuration is given. The construction and testing of the prototype are described and suggestions given for further improvements.

TABLE OF CONTENTS

LIST OF TABLES

LIST OF FIGURES

Figure Page

1. INTRODUCTION

1.1 *Global Atmospheric Electrical System*

It has been known for over two hundred years that a vertical potential gradient of about 100 V/m exists in the lowest atmosphere under fair weather conditions. It has been known for about one hundred years that the atmosphere has a finite conductivity: the time constant for loss of charge from a conductor is about 10 min. The potential gradient and conductivity lead to the conclusion that there is a current flowing down through the atmosphere and into the ground which has a density ranging from about 4×10^{-12} A/m^2 over the oceans to about 1×10^{-12} A/m^2 in cities (the difference results from the variability of conductivity associated with atmospheric pollution). Direct measurements confirm the existence of the current.

The origin of this current was first explained by *Wilson* [1920]. He suggested th storms as the electrical generators of a global atmospheric electrical system. This idea has been developed over the years and, until recently, has not met with serious objection. Critical experiments supporting the theory include the observation by *Mauchly* [1923] that the diurnal variation of potential gradient over the oceans followed Universal Time rather than local time. Subsequently *Whipple and Scrase* [1936] showed that the diurnal variation of thunderstorm activity is in phase with that of potential gradient. In another important observation *Gish and Wait* [1950], using conductivity and electric field instruments in an aircraft flown over thunderstorms, determined that the electric current at the generator was of the magnitude required by the theory.

The analysis of the global atmospheric electric system has been refined

and the present situation is best represented by the work of *Hays and Roble* [1979] and *Roble and Hays* [1979]. Their model is illustrated in Figure 1.1. In this figure Region "0" is a lower boundary of the system with local variations in atmospheric conductivity and with the varying height of the land surface included. Region "1" includes the thunderstorms as electrical generators. Region "2", above the thunderstorms, is considered not to have any driving forces and to have a conductivity which is isotropic. At higher altitudes the conductivity is anisotropic and, in addition, small electric fields are generated in the ionosphere and the magnetosphere.

The general acceptance of a global atmospheric electricity system has been complicated by recent observations of electric fields in the middle atmosphere which are greater than theory predicts. This report concerns the development of an instrument to be included in a rocket payload with the objective of establishing the existence of these anomalous electric fields.

1.2 *Middle Atmosphere Electrodynamics*

The electrical conductivity of the atmosphere increases rapidly with height. Two main factors are involved. One is the increasing mobility of the charged particles associated with the decrease of atmospheric (neutral) density and, above 60 km, the presence of free electrons. *Cole and Pierce* [1965] calculated the conductivity in the altitude range 0 to 100 km. Similar, more recent calculations by *Reid* [1979], are shown in Figure 1.2. The difference between polar and equatorial values of conductivity at altitudes below 65 km is the result of the reduced flux of cosmic rays at low latitudes.

A high conductivity implies low values of electric field, provided that the current is constant. For $\sigma = 10^{-9}$ mho/m, as near 60 km, the electric field for a current density of 2×10^{-12} A/m^2 is 2 mV/m. For

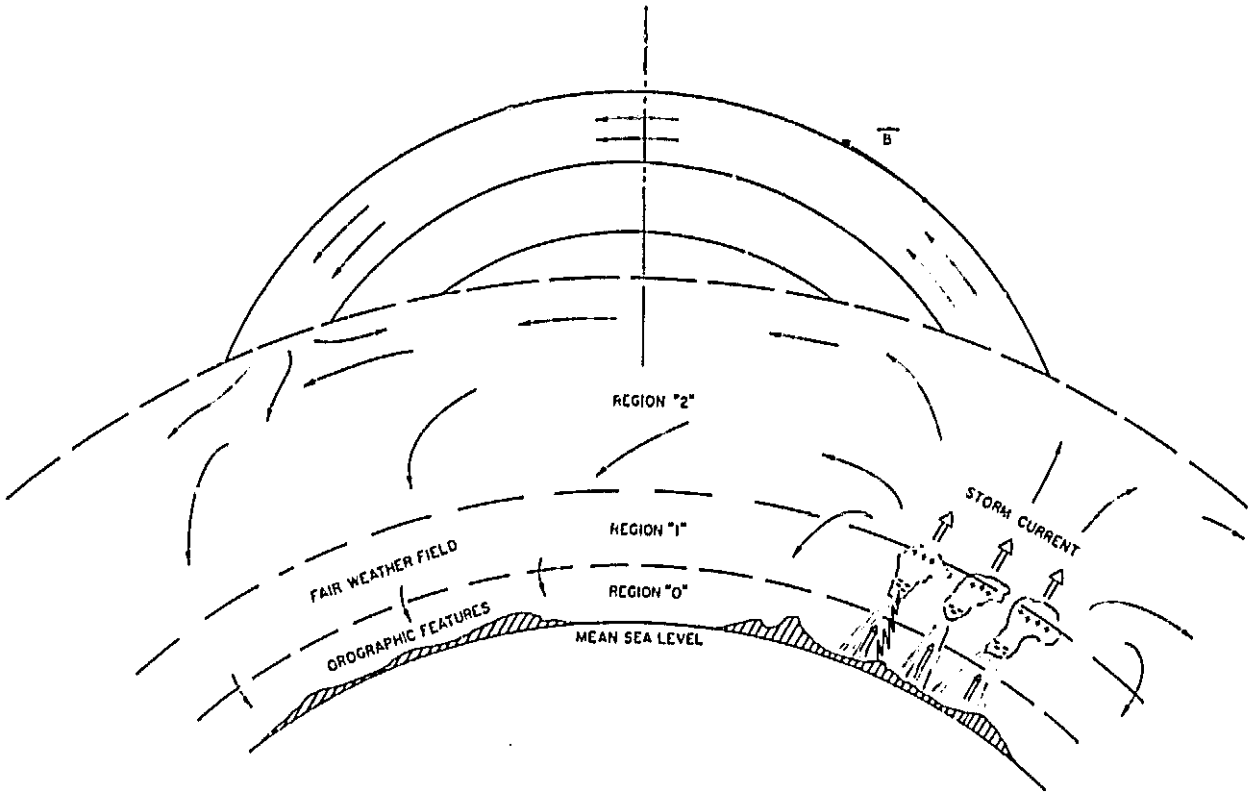

Figure 1.1 Schematic diagram of the global model of atmospheric electricity. The vector $\vec{B}$ illustrates the earth's geomagnetic field line [*Hays and Roble*, 1979].

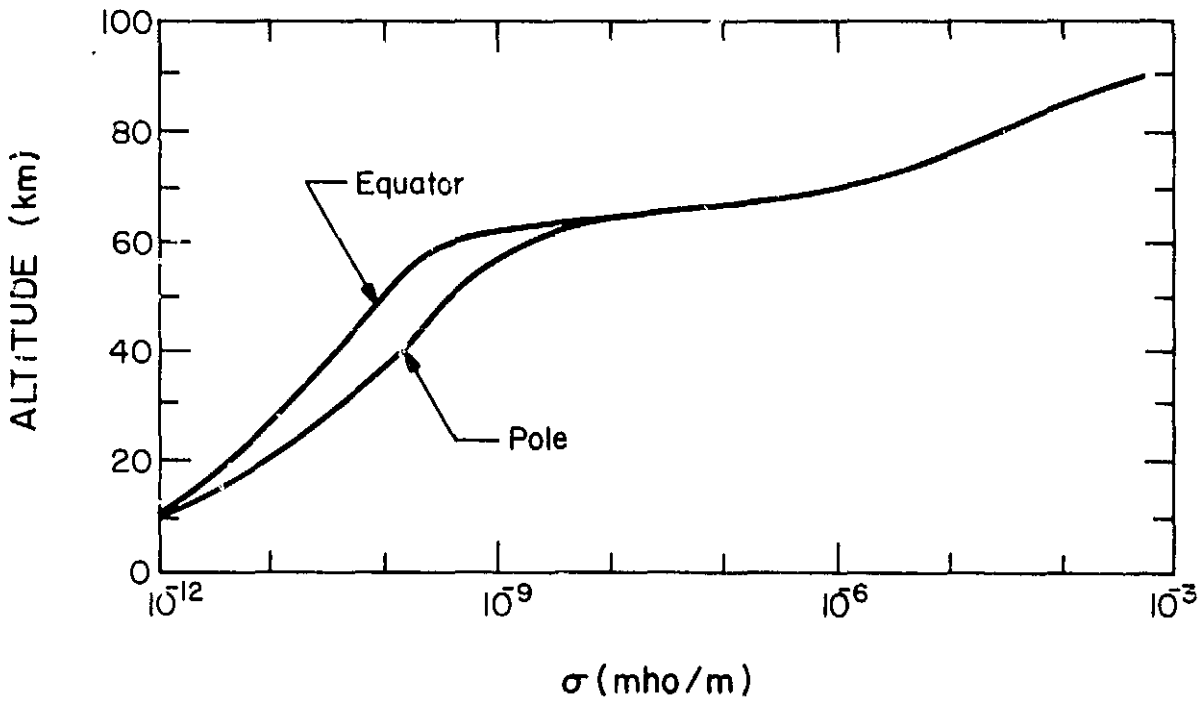

Figure 1.2 Electrical conductivity of the atmosphere between 10 and 90 km for a solar zenith angle of 45°. The latitude variation is the result of the change in cosmic ray flux. [Adapted from *Reid*, 1979]

$\sigma = 10^{-6}$ mho/m, at 70 km, the electric field would be 2 μV/m.

Bragin et al. [1974] and *Tyutin* [1976] have reported the results of rocket flights which indicate vertical electric fields, in the altitude range of 50 to 70 km, which are much greater than expected. A maximum value of 14 V/m was observed at an altitude of 57 km. *Hale and Crosby* [1979] and *Hale et al.* [1981] found evidence of a high electric field near this altitude on one rocket flight during quiet auroral conditions though it was not present on a similar flight under disturbed conditions.

Subsequent launches at middle and at high latitudes have sometimes supported the existence of the anomalous fields: *Pfaff et al.* [1980]; *Maynard et al.* [1981]; *Maynard et al.* [1982]. On the other hand, *Kelley et al.* [1982] showed that, in their own experiment, the anomalous electric field was apparently spurious, and they doubt the existence of high electric fields in the middle atmosphere.

If the phenomenon is real then the most obvious explanation is that it results from a lower-than-normal conductivity. However low conductivity values are not supported by direct observation [*Hale et al.*, 1981] and, in any case, this explanation would exchange one anomaly for another.

Apart from the intrinsic interest these high electric fields near 60 km are important as a transport mechanism for ionization and must be investigated.

Two substantially different types of instruments are available for measuring electric fields in the atmosphere. In regions of high conductivity (as in the ionosphere and magnetosphere) the double floating probe (for example, *Mozer* [1971])has proved effective. The potential difference between two probes is measured by a circuit which is, in effect, a high impedance voltmeter. With a known distance separating the probes the electric field is simply derived.

Where the conductivity is low (as in the troposphere and stratosphere) the probe-type experiment can be used although the conductivity adjacent to the probe must be artificially increased, generally by use of a radioactive source. This approach is not suitable for an aeroplane or rocket and the preferred technique uses electrostatic induction, rather than electrical conduction. This type of instrument is commonly known as a field mill.

In the altitude range of particular interest here (50 to 70 km) both types of instrument are possible though both are at the limit of their useful range of altitude. The instrument used by *Bragin et al.* [1974] and *Tyutin* [1976] appears to be a composite of the two types, which makes the interpretation of the data rather complex.

The recent rocket flights of *Maynard et al.* [1982] and of *Kelley et al.* [1982] have used the double-probe technique with no clear confirmation of the existence of high middle-atmosphere electric fields. Since this may be a limitation by the experiment it is planned to measure the middle-atmosphere electric field using an induction type of instrument.

1.3 *Outline of Report*

The preceding sections have given a discussion of mesospheric electric fields and explained why an alternative method of measuring electric fields is desirable. Each of the following parts of this report deals with a specific aspect of the electric field meter. Chapter 2 contains a theoretical discussion of the experiment followed by a general description of the system. Chapter 3 contains a detailed description of the electronic circuits used to implement the electric field meter while Chapter 4 discusses the mechanical design of the system. This chapter also specifies the power requirements and the proposed flight configuration. Testing and calibration are described

in Chapter 5. This chapter also serves as an operator's manual. Chapter 6 contains suggestions for future improvements.

2. DESIGN CONSIDERATIONS

2.1 *Theoretical Analysis*

The electric field meter is designed to operate in the middle atmosphere where the conductivity of the medium cannot be ignored, and, in fact, can usefully be measured. This is accomplished in the instrument by separately sensing the displacement current and the conduction current into the sensor.

Equation (2.1) gives the surface charge density (C/m^2) of a metal plate in an electric field E (V/m)

$$\sigma = -\varepsilon_o E \tag{2.1}$$

where $\varepsilon_o = 8.85 \times 10^{-12}$ F/M.

The charge Q (C) on a plate of area A (m^2) is thus

$$Q = -\varepsilon_o EA \tag{2.2}$$

In the electric field meter the plate (stator) is cyclically covered and uncovered by a grounded plate (rotor) so that the exposed area of the stator is a function of time A(t). Then the induced charge is also a function of time

$$Q(t) = -\varepsilon_o EA(t) \tag{2.3}$$

The stator is connected to a current-measuring device. The current, which is a displacement current, is

$$i_d(t) = \frac{dQ(t)}{dt} = -\varepsilon_o E \frac{dA(t)}{dt} \tag{2.4}$$

If the ambient medium has finite conductivity then there is also a conduction current into the stator

$$i_c(t) = \lambda_p A(t)E \tag{2.5}$$

where λ_p is the polar conductivity for positive or negative ions (for positive

or negative electric fields, respectively).

Since it is desired to measure both the displacement and conduction currents, and since the displacement current is proportional to the derivative of the area while the conduction current is directly proportional to the area, a sinusoidal area function allows the two components to be separated using phase-sensitive detection.

Letting the area function be

$$A(t) = A_o(1 + \sin\omega t) \tag{2.6}$$

where A_o is a constant (equal to half of the maximum exposed area of the stator), one obtains conduction and displacement currents varying at the same frequency. Substituting equation (2.6) into equations (2.4) and (2.5) and performing the derivative operation in equations (2.4), one obtains

$$i_d(t) = -\varepsilon_o E A_o \omega \cos\omega t = i_{dm} \cos\omega t \tag{2.7}$$

$$i_c(t) = \lambda_p E A_o (1 + \sin\omega t) = i_{cm}(1 + \sin\omega t) \tag{2.8}$$

Combining equations (2.7) and (2.8) an equation which relates the total current to the atmosphere's conductivity and electric field is derived

$$i(t) = i_d(t) + i_c(t) = i_{dm} \cos\omega t + i_{cm}(1 + \sin\omega t) \tag{2.9}$$

The circuit measures the AC component of this current

$$i_{ac}(t) = i_{dm} \cos\omega t + i_{cm} \sin\omega t \tag{2.10}$$

Using the identity

$$M\cos(\omega t - \phi) \equiv M\cos\omega t \cos\phi + M\sin\omega t \sin\phi \tag{2.11}$$

where M is a constant, and then comparing equations (2.10) and (2.11) one sees that

$$i_{dm} = M\cos\phi \tag{2.12}$$

$$i_{cm} = M\sin\phi \tag{2.13}$$

If the magnitude (M) and phase (ϕ) of the ac current into the stator are measured, then the magnitude of the conduction current (i_{cm}) and the displacement current (i_{dm}) can be obtained from equations (2.12) and (2.13). Once i_{dm} is determined the electric field is calculated using equation (2.7)

$$E = -i_{dm}/\varepsilon_o A_o \omega \tag{2.14}$$

where ε_o, A_o, and ω are known constants.

Knowing both i_{dm} and i_{cm}, equation (2.8) is used to obtain the polar conductivity

$$\lambda_p = i_{cm}/EA_o = \varepsilon_o \omega (i_{cm}/i_{dm}) \tag{2.15}$$

2.2 *Implementation of Sinusoidal Area Function*

The previous section presented a method by which one can obtain the atmospheric electric field and the conductivity; a method which relies on using a sinusoidal varying area function. In this section, the design of the rotor and stator to implement this sinusoidal variation in area is discussed.

It is assumed that the rotor sweeps out an area defined by a rotating radius from its center. This is actually the edge of a sector in the rotor. Then, in polar coordinates the area swept out by the rotor is given by

$$A(\theta) = \int_o^\theta \tfrac{1}{2} r^2 \, d\theta \tag{2.16}$$

Let the radius be

$$r = R\sqrt{\sin C\theta} \tag{2.17}$$

where R is a constant, actually the maximum stator radius, and C is equal to the number of segments. The area function becomes

$$A(\theta) = \int_o^\theta \tfrac{1}{2} R^2 \sin C\theta \, d\theta \tag{2.18}$$

On integration, and ignoring the minus sign, one finds

$$A(\theta) = (R^2/2C)\cos C\theta \tag{2.19}$$

A modification which must be taken into account arises from the fact that the rotor shaft must pass through the stator. Equation (2.17) implies that the radius is zero when $C\theta$ is equal to zero, but, since the center of the stator is, in practice, occupied by the rotor shaft, the radius cannot be zero. To overcome this, the radius function must be greater than or equal to a constant determined by the radius of the rotor shaft. This may be accomplished by modifying equation (2.17) to

$$r = \sqrt{R^2 \sin C\theta + r_{min}^2} \tag{2.20}$$

where r_{min} is the minimum radius of the stator and R is a new constant.

The area of an individual segment of the stator is then equal to the area bounded by the outer radius, given by equation (2.20), and the inner radius, the radius of the hole made for the rotor shaft. The segment area is thus

$$A(\theta) = \int_0^\theta \tfrac{1}{2} (R^2 \sin C\theta + r_{min}^2)d\theta - \int_0^\theta \tfrac{1}{2} (r_{min}^2)d\theta \tag{2.21}$$

This simplifies to

$$A(\theta) = \int_0^\theta \tfrac{1}{2} R^2 \sin C\theta \, d\theta \tag{2.22}$$

which is the same as equation (2.18).

The limits of integration are now set such that the integration is performed over the positive half of the sine function: $C\theta = 0$ to $C\theta = \pi$. This corresponds to the times when the area function goes from a minimum to a maximum; the time during which the stator is completely shielded by the rotor to the time when the stator is fully exposed. As $C\theta$ goes from π to 2π, the area

function sinusoidally decreases as the rotor begins to cover the stator. The total area of one segment of the stator is, thus,

$$A = R^2/C \tag{2.23}$$

The total area of the stator is the number of segments, C, multiplied by the area one segment, R^2/C, and is therefore equal to R^2. The value of R is now derived as follows. Given the maximum allowable radius of the stator, r_{max}, and the minimum radius, r_{min}, one can use equation (2.20) to determine R. From this equation r_{max} occurs when $C\theta$ is equal to zero. Thus

$$r_{max} = \sqrt{R^2 + r_{min}^2} \tag{2.24}$$

which, on rearranging, gives

$$R^2 = r_{max}^2 - r_{min}^2 \tag{2.25}$$

This equation shows, interestingly, that the total stator area (R^2) is a function of r_{max} and r_{min} but not a function of C, the number of segments.

In summary, to obtain an area function of the form

$$A = A_o(1 + \sin\omega t) \tag{2.26}$$

the radius of the stator, as a function of rotation angle, is

$$r = \sqrt{(r_{max}^2 - r_{min}^2)\sin C\theta + r_{min}^2} \tag{2.27}$$

where r_{max} is the maximum radius of the stator, r_{min} is the radius of the hole in the stator to allow for rotor shaft clearance, and C is the number of segments.

Table 2.1 presents a program for a TI-58 hand-held calculator which can be used to plot equation (2.27) and also calculate the stator area, given values of r_{max}, r_{min}, and C. Table 2.2 gives the operating sequence of this program.

Table 2.1 TI-58 program to calculate the stator radius in polar co-ordinates and to calculate the total stator area.

Memory location 00 : r_{max}, maximum allowable stator radius

Memory location 01 : r_{min} minimum radius of stator

Memory location 02 : C, number of segments

Memory location 03 : R^2, total stator area

Memory location 04 : θ, in degrees

STEP	KEY	KEY CODE	COMMENTS
000	STO	42	Store θ
001	04	04	
002	RCL	43	Compute stator area
003	00	00	Using equation (2.25)
004	X^2	33	and store result
005	-	75	in location 03
006	RCL	43	
007	01	01	
008	X^2	33	
009	=	95	
010	STO	42	
011	03	03	
012	RCL	43	Compute r using
013	04	04	equation (2.27)
014	x	65	
015	RCL	43	
016	02	02	
017	=	95	
018	2nd sin	38	
019	x	65	
020	RCL	43	
021	03	03	
022	+	85	
023	RCL	43	
024	01	01	
025	X^2	33	
026	=	95	
027	$\sqrt{\ }$	34	
028	R/S	91	
029	RST	81	Display r
030	LRN	--	
031	RST	--	

Table 2.2 Operating sequence for running the stator-radius program.

1. Enter program as listed in Table 2.1
2. Store r_{max} in memory location 00
3. Store r_{in} in memory location 01
4. Store C in memory location 02
5. Enter θ in degrees. Press R/S key. Calculator will display r.
6. Repeat step 5 for different values of θ
7. Stator area is stored in memory location 03

Figure 2.1 shows the four-segment stator used in the instrument. The total area is 13.3 cm^2 with r_{max} = 1 15/32 in. (37.30 mm) and r_{min} = 5/16 in. (7.94 mm).

The finished transducer is shown in Figure 2.2. The rotor and stator are visible at the top of the instrument.

2.3 *General Description of System*

The field mill transducer produces a sinusoidal variation in the exposed area on the stator. The signal developed on the stator is amplified, and as indicated in Figure 2.3, the magnitude and phase of the signal are determined separately.

The arrangement of the instrument is shown in more detail in Figure 2.4. A chopper disc and optical switch are used to generate a phase reference signal. The figure also includes a speed control for the motor. This was initially considered desirable but was not implemented when it was found that the measurements are not sensitive to motor speed variations.

The transducer, shown in Figure 2.2, houses the preamplifier, the motor and the optical switch. The other parts of the system are contained in the signal processing unit.

Connections between the field mill transducer and the signal processing unit are made possible by an eight-line cable originating from the former. This cable terminates on the top side of the signal processing unit. Two of the three circuit cards, the magnitude detector and the phase detector circuits, are contained in this unit together with the voltage regulators.

The system produces two outputs representing magnitude and phase. Both signals are conditioned to fall in the range 0 to 5 V in order to be compatible with the FM/FM telemetry system of the payload.

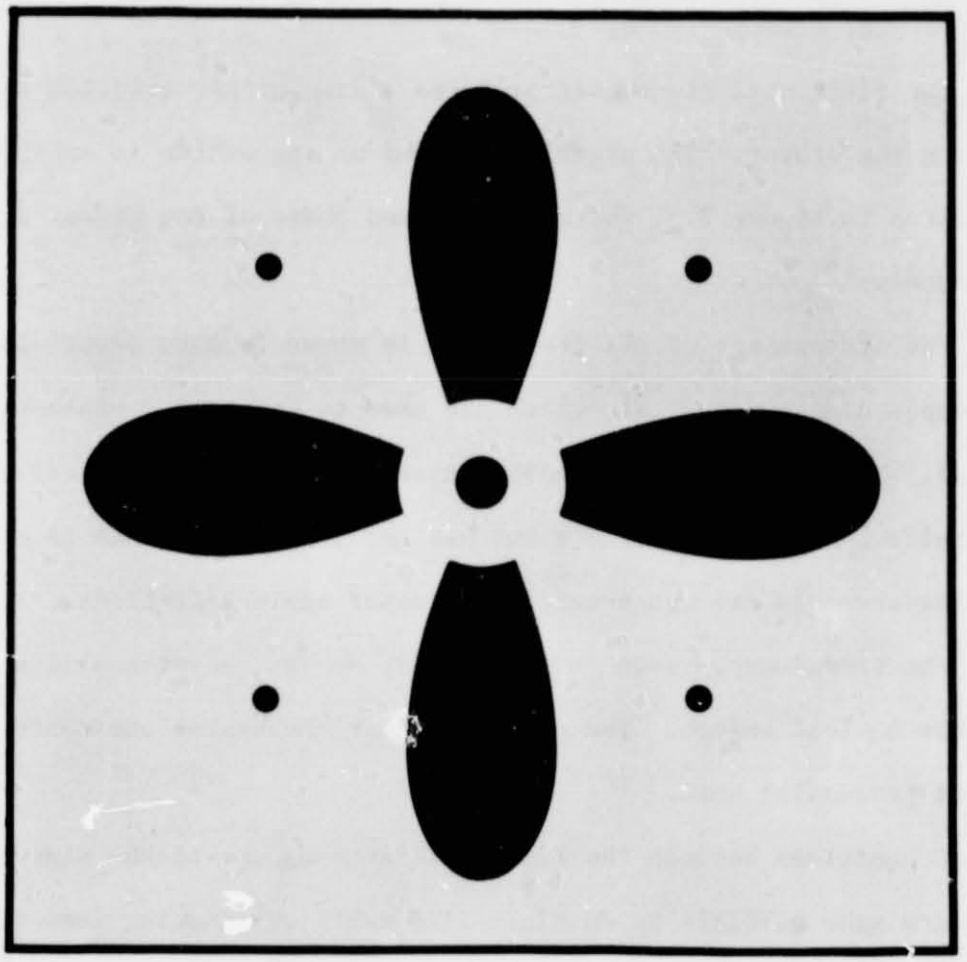

Figure 2.1 Prototype stator designed from equation (2.27) with r_{max} = 37.30 mm, r_{min} = 7.94 mm and C = 4. The stator is constructed on a printed circuit board.

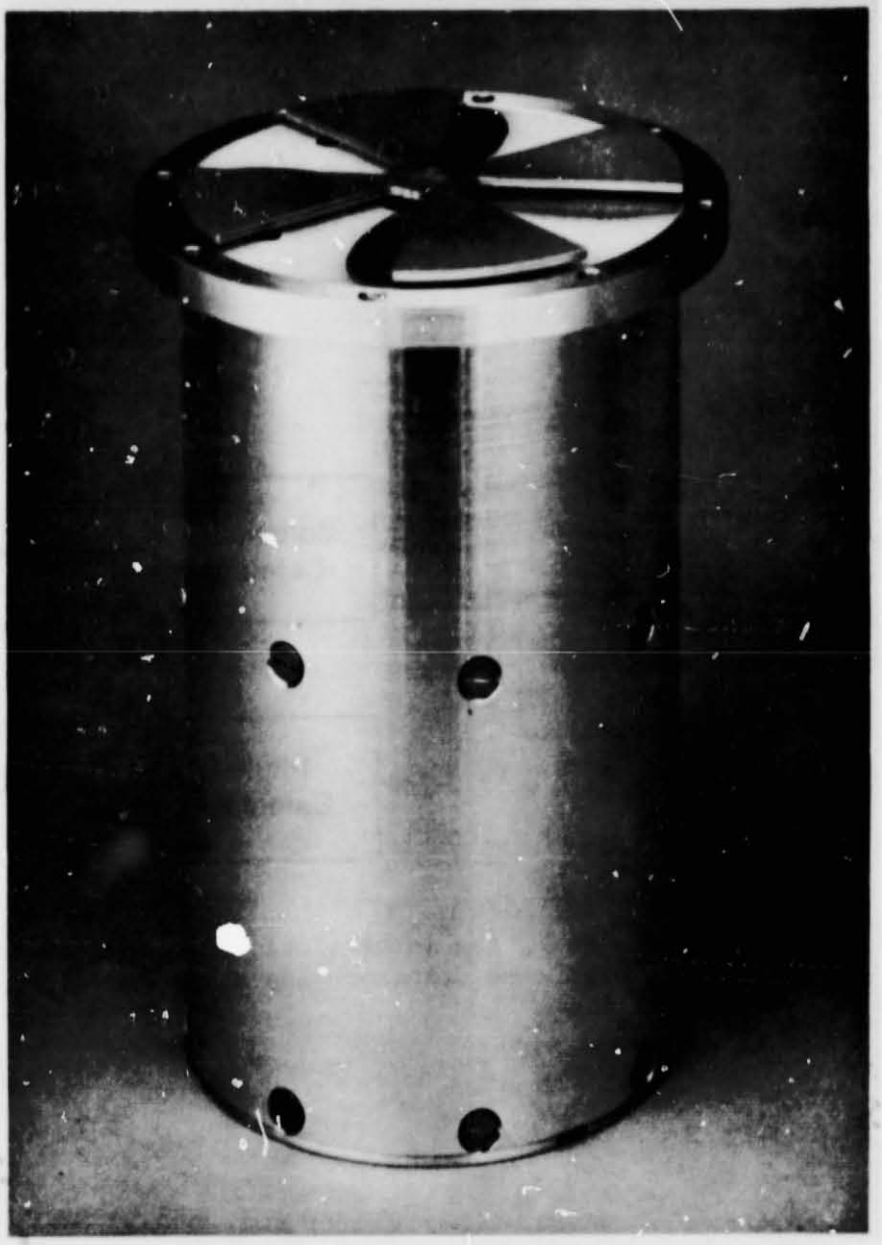

Figure 2.2 The transducer showing the rotor and stator. Excluding the rotor the overall length is 5 in. (127 mm).

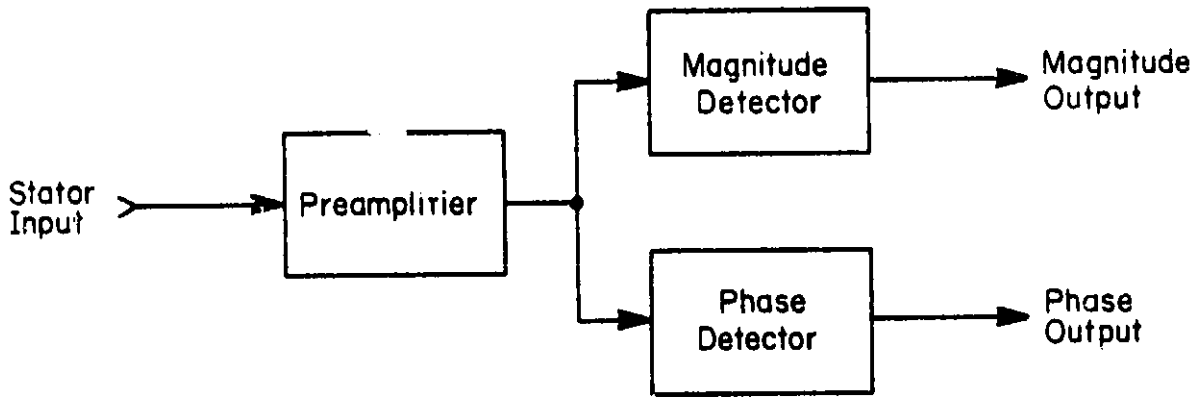

Figure 2.3 Block diagram showing the interrelationship between the stator, preamplifier, magnitude detector and phase detector.

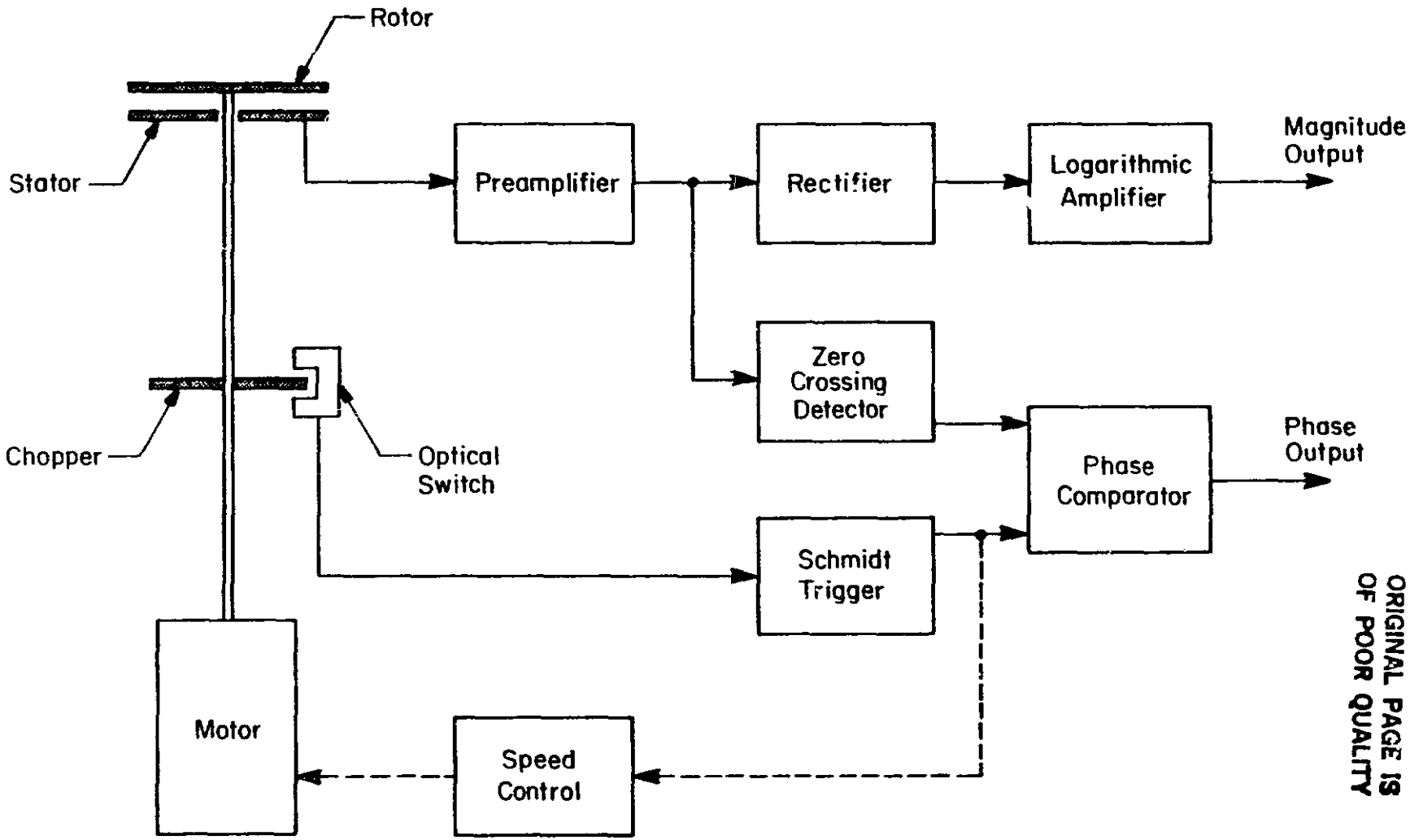

Figure 2.4 Block schematic of the electric field meter including an optional speed control.

The magnitude of the ac signal into the stator is determined, after sufficient amplification, by rectification. The dymanic range of the instrument is extended to four decades by logarithmic compression of the signal.

The phase output is also designed to respond to signals which vary in magnitude over four decades. The phase difference between the two signals is then determined using a six-state asynchronous sequential network.

The details of these circuits are given in subsequent chapters.

2.4 *System Specifications*

2.4.1 *Altitude range.* In the lowest atmosphere because of the low value of conductivity the conduction current is negligible compared with the displacement current. At a sufficiently great altitude the conduction current is equal in magnitude to the displacement current. The two components of the current do, however, differ in phase by 90° which allows them to be measured separately. In fact it would appear possible to detect a displacement current which is somewhat smaller than the conduction current.

The upper limit of altitude at which the induction type of field meter can be expected to give useful information will now be derived. From equation (2.7) the peak value of the displacement current is

$$i_{dm} = \varepsilon_o E A_o \omega \tag{2.28}$$

Also, from equation (2.8) the peak value of the ac component of the conduction current is

$$i_{cm} = \lambda_p E A_o \tag{2.29}$$

The ratio of the magnitudes is

$$i_{dm}/i_{cm} = \varepsilon_o \omega/\lambda_p \tag{2.30}$$

The conductivity near the ground, in unpolluted regions, is about 2×10^{-14} mho/m so that the polar conductivity is about 1×10^{-14} mho/m (the

mobilities of the positive and negative ions are nearly equal). Thus for measurements in the lower atmosphere the conduction current is less than the displacement current by a factor of about 10^6, for an operating frequency of 100 Hz.

For the same operating frequency the ratio has the value unity for

$$\lambda_p = \varepsilon_o \omega = 6 \times 10^{-9} \text{ mho/m} \tag{2.31}$$

From Figure 1.2 the two components are thus equal in magnitude at an altitude of about 64 km. It is reasonable to expect that, under favorable conditions, phase detection would allow measurement of a displacement current smaller than the conduction current. Taking 0.1 for the ratio i_{dm}/i_{cm}, the polar conductivity, from equation (2.30) is 6×10^{-8} mho/m. This occurs at an altitude (again using Figure 1.2) of about 67 km. Thus the experiment is valid for altitudes up to 67 km.

2.4.2 *Magnitudes of currents.* Using a stator area of 13.3 cm^2 and an operating frequency of 100 Hz the peak value of the displacement current is, from equation (2.28),

$$i_{dm} = 3.7 \times 10^{-12} \text{ E} \tag{2.32}$$

Thus the peak displacement current is 3.7 pA for an electric field of 1 V/m. It is desired to measure electric fields of the order of 1 V/m so that, as an absolute minimum, the displacement current should be measured to an accuracy of 1 pA.

Measurement of such a small ac current presents considerable experimental difficulty but, as will be seen later, a practical system can be built. It is likely that even smaller electric fields can be measured with further refinements in the system.

2.4.3 *Configuration.* The signal to be measured is proportional to the area of the stator. Thus the largest possible area should be used for maximum sensitivity. The size is, however, limited by the payload into which the instrument will be incorporated. To allow for the possibility of flight in a 6.5 in (165 mm) diameter payload (as for a Nike Apache) the overall length of the transducer is set at 5 in (127 mm). With this dimension the maximum diameter of the stator is 3 in (76 mm). This leads to 13.3 cm^2 as the maximum stator area for the sinusoidal area function (section 2.2).

2.4.4 *Operating frequency.* The amplitude of the displacement current is, from equation (2.7), proportional to the frequency of the ac signal. This, in turn, is established by the motor rotational speed and the number of segments in the stator. It is advantageous to increase the operating frequency to the maximum practical value; this increases the magnitude of the displacement current.

The number of stator segments was chosen to be four. A larger number could be used, perhaps up to eight, but a study would be necessary of the limitation placed by edge effects (fringing fields).

The motor chosen for the prototype instrument has a no-load speed of 5250 rpm at the working voltage of 12 V. Thus, at the maximum motor speed, the operating frequency is 350 Hz. In order to conserve power the operating speed was finally chosen to be 100 Hz.

It will be seen later (section 5.1.2) that a limitation is placed on the ability to measure small currents by the modulation of rotor-stator capacitance. This gives rise to an unwanted signal, another ac displacement current, which has an amplitude proportional to the operating frequency.

Thus, although the preamplifier requirements would be considerably eased by use of a higher operating frequency of, say, 1 kHz, there would be no improvement in the limit of detectability of the ambient electric field.

3. ELECTRONIC CIRCUITS

3.1 *Preamplifier*

The preamplifier is a critical component in the electric field meter. It is required to convert ac currents in the range 1 pA to 1 nA to voltages in the range 5 mV to 5 V. Figure 3.1 is a block diagram of the preamplifier which contains three operational amplifiers.

The sensitivity of the preamplifier is largely determined by the first stage. This uses the AD515J, a precision, low-power, FET-input electrometer operational amplifier. Among the more prominent characteristics of the device are:

Input bias current: 0.3 pA, maximum

Input current noise: 0.01 pA rms for 10 Hz to 10 kHz

Input offset voltage: 3 mV, maximum; 0.4 mV, typical

Input offset voltage drift: 50 μV/°C, maximum

Referring to Figure 3.2, since the inverting input is at virtual ground, the input current (I) flows through the feedback resistor R101 to the output producing an output voltage given by

$$V = -IR_{101} \tag{3.1}$$

The feedback resistor is chosen to be 10^9 Ω so that the sensitivity of the stage is 1 mV/pA. C101 is used to stabilize the op amp and also set a high frequency cutoff:

$$f_c = \frac{1}{2\pi C_{101} R_{101}} \tag{3.2}$$

Letting C101 equal 1 pF, the cutoff frequency becomes 160 Hz, 60 Hz above the operating frequency of 100 Hz.

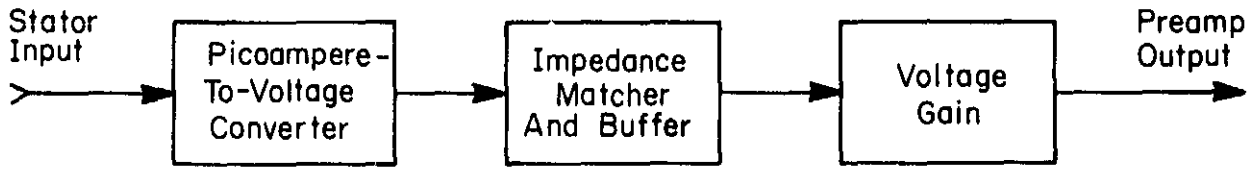

Figure 3.1 Block schematic of the preamplifier.

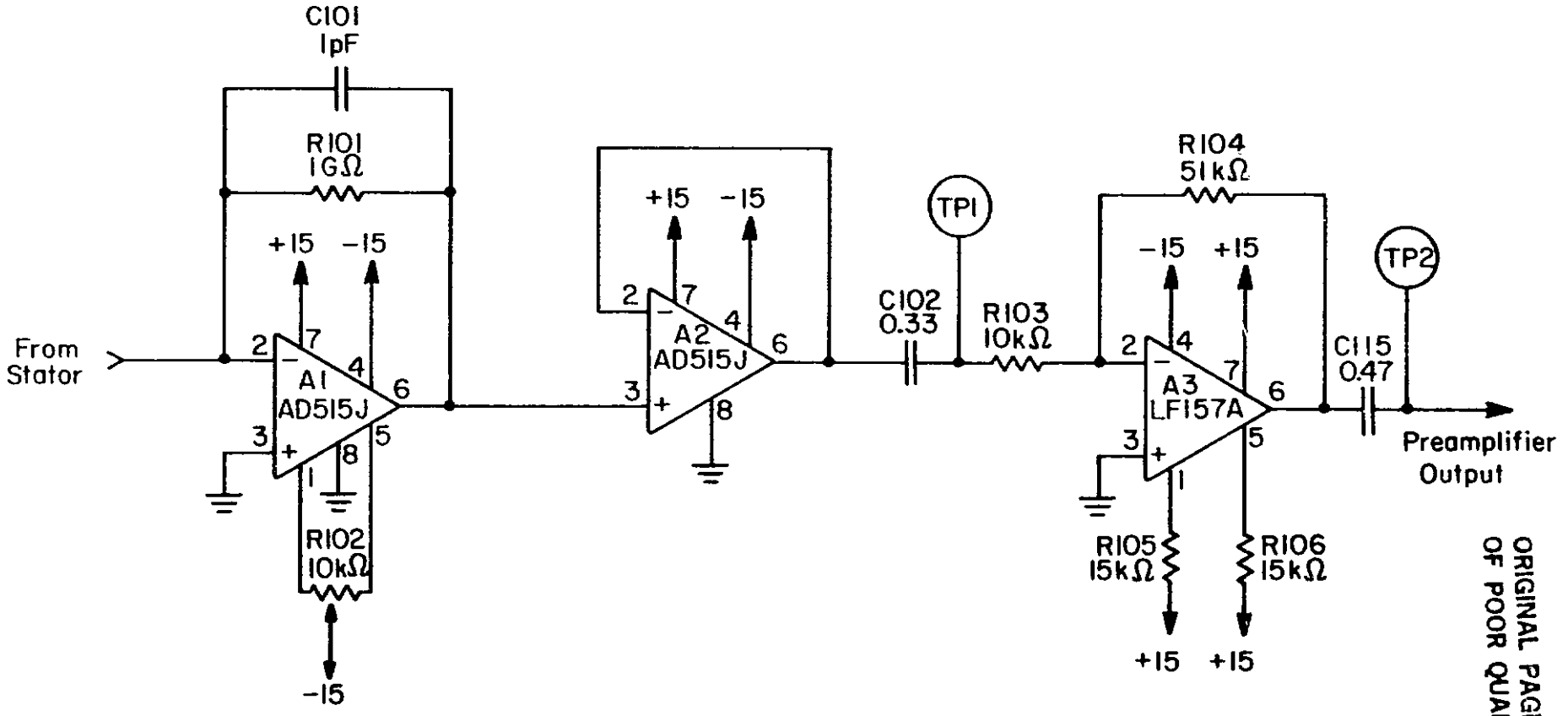

Figure 3.2 Circuit of the preamplifier.

The current-to-voltage converter is followed by a voltage follower. A second AD515J operational amplifier is used.

The output of the voltage follower is connected to an amplifier by capacitor C102. With R103 this gives a lower 3 dB frequency of 50 Hz, blocking the dc component of the conduction current and improving the signal-to-noise ratio in the system.

The amplifier is used to boost the signals appearing at test point 1 into voltages suitable for the magnitude and phase detector circuits: mainly $2\ mV \leq V \leq 15\ V$ (peak values). A National Semiconductor LF157 is used in an inverting configuration. The particular device is chosen primarily for its small input offset voltage (1 mV), and secondarily for its low input-noise voltage ($12\ nV/\sqrt{Hz}$) and low input-offset-voltage temperature drift (3 μV/°C). Although the picoampere-to-voltage converter is designed to operate with inputs in the range of 1 pA to 15 nA, corresponding to outputs, of that stage, in the range of 1 mV to 15 V, setting the gain of the LF157 at five has a definite advantage. The 1 mV output of the picoampere-to-voltage converter is increased to 5 mV, a voltage which falls in the acceptable input voltage range for the magnitude and phase detector circuits. The additional gain reduces the maximum input signal that can be accommodated to 3 nA. However this is of no consequence for the expected range of electric field values in the middle atmosphere.

Using a calibration procedure to be described later (section 3.5) it is verified that there is a linear relationship between input current and output voltages. The theoretical relationship is

$$V_o = 5 \times 10^9 \, I \qquad (3.3)$$

As illustrated in Table 3.1 the actual output voltages are 10 percent larger than the theoretical values. This is attributable to component tolerance: no attempt was made to set the gain to a precise value.

3.2 *Magnitude Detector*

3.2.1 *Introduction.* The magnitude detector of the electric field meter is designed with the following constraints:

1. The input is a sinusoidal signal with a frequency of 100 Hz.
2. The input voltage range is 5 mV to 15 V (peak value).
3. The output voltage range is 0 to 5 V.

The circuit implementation of the magnitude detector is divided into three main parts: a RMS-to-dc converter, a log amplifier and an output amplifier, shown in Figure 3.3. The complete circuit is shown in Figure 3.4.

3.2.2 *RMS-to-dc converter.* The RMS-to-dc converter is the Analog Device AD536A. The output voltage of this device is the true RMS value of the input voltage and it can be used with any type of input signals; sinusoidal, triangular, or even ramp functions. C103 (Figure 3.4) at pin 4 of the device is the averaging capacitor. Chosen for the operating frequency of 100 Hz, this 1 μF capacitor ensures that the dc output error is less than 0.5% of the reading. Moreover, the device has a two pole active filter on the output to reduce the ac ripple on the output. Choosing C104 and C105 to be 2.2 μF and R107 to be 24 kΩ, the ac peak-to-peak ripple is reduced to approximately 0.05% of the output reading. Testing the circuit with a 100 Hz

Table 3.1 Calibration of the preamplifier for a 100 Hz sinusoid. Currents and voltages are peak values.

Input (pA)	Theoretical V_o	Actual V_o	Ratio Act/Th
1	.005	-	-
3	.015	.016	1.1
6	.030	.033	1.10
10	.050	.055	1.10
30	.150	.165	1.10
60	.300	.333	1.11
100	.500	.552	1.104
300	1.500	1.650	1.100
600	3.000	3.300	1.100
1000	5.000	5.480	1.096
3000	15.000	16.450	1.096

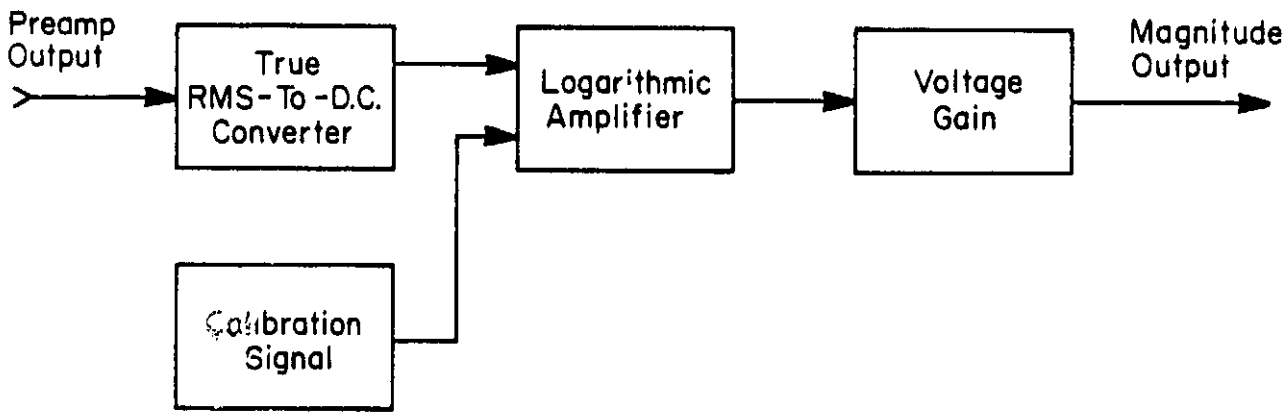

Figure 3.3 Block schematic of the magnitude detector.

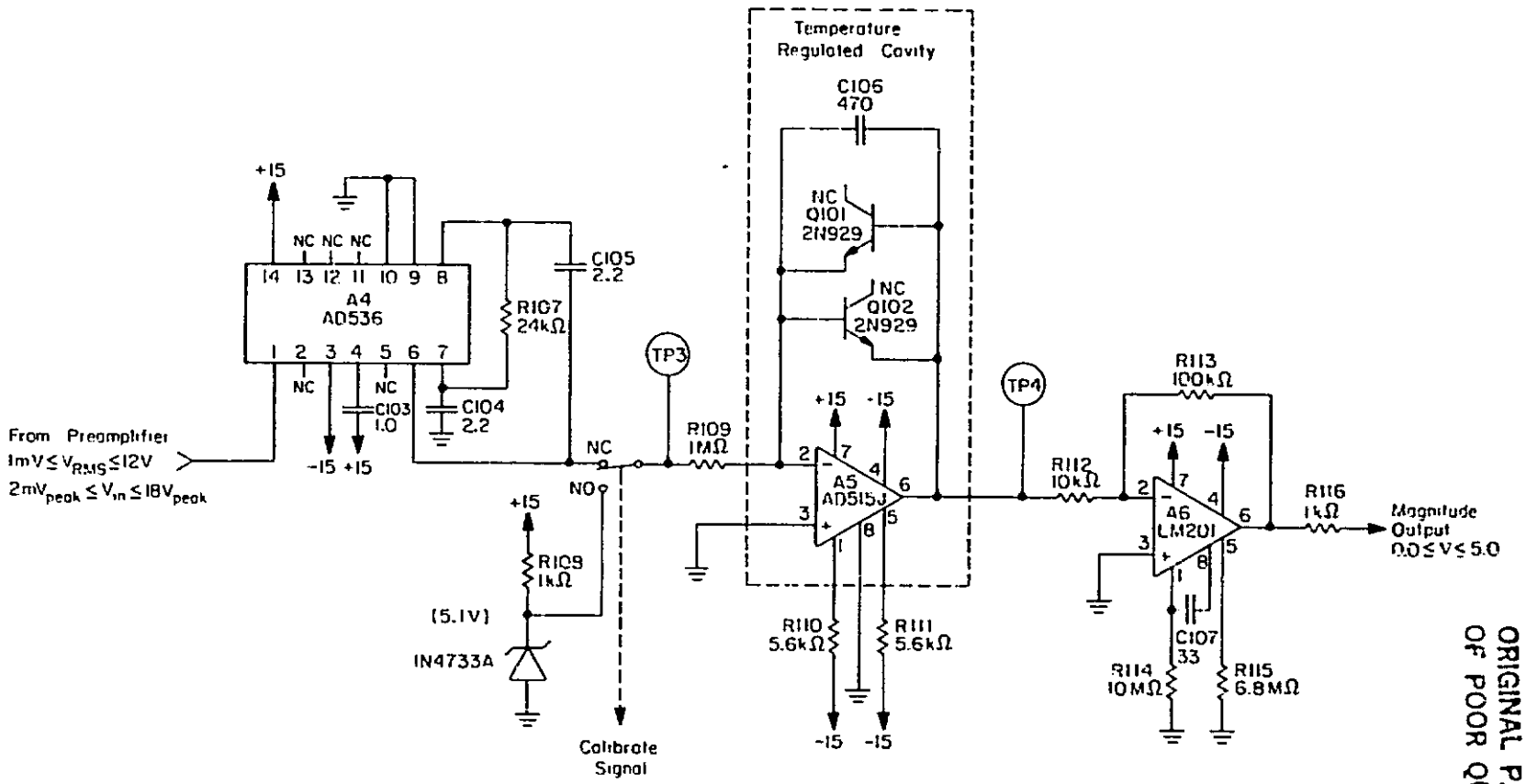

Figure 3.4 Circuit of the magnitude detector. Dotted line indicates that portion of the circuit which is enclosed within the temperature-regulated cavity.

sinusoidal input confirmed these claims.

3.2.3 *Logarithmic amplifier.* The output of the RMS-to-dc converter is connected to the logarithmic amplifier. Referring to Figure 3.4 a voltage at test point 3 creates a current through resistor R109 (the inverting input of the operational amplifier is at virtual ground). This current then flows through one of the diodes in the feedback loop (which diode depends on the polarity of the signal). The base-emitter junction of 2N929 transistors is used as diodes since they provide small reverse leakage currents (2.5 pA) and low noise operation. It was found that the logarithmic amplifier had a more nearly linear response when the collector junction of the transistors was left open compared with the usual practice of tying the collector to the base.

The diode equation is

$$I = I_o(e^{V/V_T} - 1) \tag{3.4}$$

where I_o is the reverse leakage current and $V_T = kT/q$. Both I_o and V_T vary with temperature. In order to remove this temperature dependence in the logarithmic amplifier the unit is sealed in a temperature-regulated cavity which is set to operate at 150 °F (340°K). For this temperature $V_T = 29.2$ mV.

Rearranging equation (3.4), one gets an expression relating the voltage across the diode to the current flowing through it

$$V = V_T \ln[(I - I_o)/I_o] \tag{3.5}$$

Since I equals the voltage at test point 3 (Figure 3.4) divided by R109 (10^6 Ω), one ultimately gets an expression relating the input voltage to the output voltage of the logarithmic amplifier. Note that the output voltage will be inverted since the inverting input of the operation amplifier is used.

Using V_T = 0.0292 V and $I_o = 2.5 \times 10^{-12}$ A one thus obtains for the transfer characteristic of the log electrometer

$$V_{OUT} = - 0.0292\ Ln[(10^6\ V_{IN} - 2.5)/2.5] \qquad (3.6)$$

Table 3.2 gives a theoretical calibration for the logarithmic amplifier operating at 150°F.

The sensitivity of a logarithmic amplifier is limited by the leakage current of the feedback diodes and/or the bias current of the operational amplifier, whichever is greater. An Analog Device AD515J operational amplifier was selected since it has an input bias current of 0.3 pA. Thus the sensitivity is here limited by the leakage current (2.5 pA) of the feedback diode.

Capacitor C106 (Figure 3.4) in the feedback loop is used to stablize the circuit's operation. The capacitor was experimentally chosen to be 470 pF to prevent oscillations. A thermal test chamber was then used to observe the logarithmic amplifier's performance at various temperatures; the test data are presented later (section 3.6).

As previously mentioned, the unit is set to operate at 150°F. This temperature was chosen for two reasons. First, since it is simpler to heat a temperature regulated cavity (using a power resistor) than to cool it, a high temperature should be selected. Second, the operating temperature should be set well above the maximum temperature the device could reach. For example, if the payload is left on a launch pad for an extended period of time, the temperature might exceed the preset operating temperature - thus defeating the purpose of the temperature regulated cavity. For these reasons, the temperature was selected to be 150 °F (65.6°C) since this is well above the expected temperature range and below the maximum operating temperature of the

Table 3.2 Theoretical calibration of the logarithmic amplifier for a temperature of 150°F.

V_{IN} (V)	V_{OUT} (V)
10.000	-.444
6.000	-.429
3.000	-.409
1.000	-.377
0.600	-.362
0.300	-.342
0.100	-.309
0.060	-.295
0.030	-.274
0.010	-.242
0.006	-.227
0.003	-.207
0.001	-.175

operational amplifier and the transistors.

3.2.4 *Temperature regulated cavity.* The temperature regulated cavity along with the associated electronics is shown in Figure 3.5. An aluminum cavity was made to cover the operational amplifier, the feedback diodes, the feedback capacitor and an Analog Device AD590 (a two terminal IC temperature transducer). This last device has a linear output of 1 μV/°K as shown in Figure 3.6.

A voltage is produced at inverting input of the comparator (A16) by routing this current through resistor R128 (Figure 3.5). C110 is placed in parallel with this resistor for stability. At the non-inverting input of the comparator is a reference voltage which sets the temperature of the cavity.

The procedure to set the temperature is as follows. Specifying a temperature of 150°F (340°K) yields a current of 340 μA from the AD590. This current flows through resistor R128 yielding a voltage (which was measured to be 3.49 V) at the inverting input of A16. Therefore, to regulate the temperature to 150°F one needs a stable voltage of 3.49 V at the non-inverting input of the comparator. This voltage is obtained by the circuit in Figure 3.5. The 3.9 V zener diode eliminates the possibility that fluctuations on the 15 V supply line will reach the comparator. A 1N757 diode is used to reduce the zener voltage to the required 3.49 V. The resistor R129 is tied between the non-inverting input of the comparator and ground to provide a path for current to flow through the diode.

The comparator used is the Data Acquisition DA462 operational amplifier. This device provides the necessary sensitivity and output driving requirements needed. The output of the DA462, which swings from +12 V to -12 V, is limited by a 1N914 diode to protect the driving transistor Q103 from a

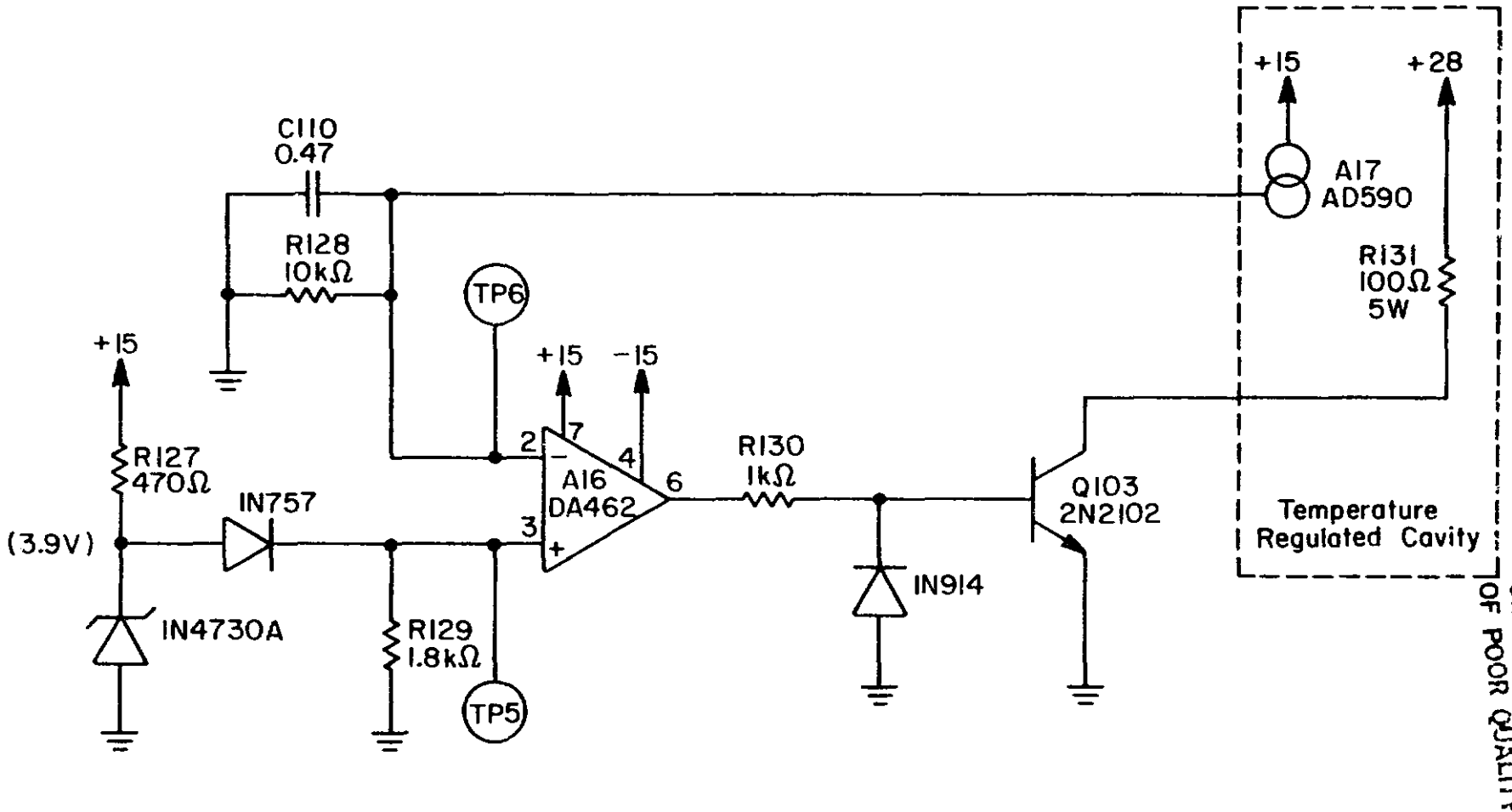

Figure 3.5 Schematic of circuit used to regulate the temperature of the temperature-regulated cavity.

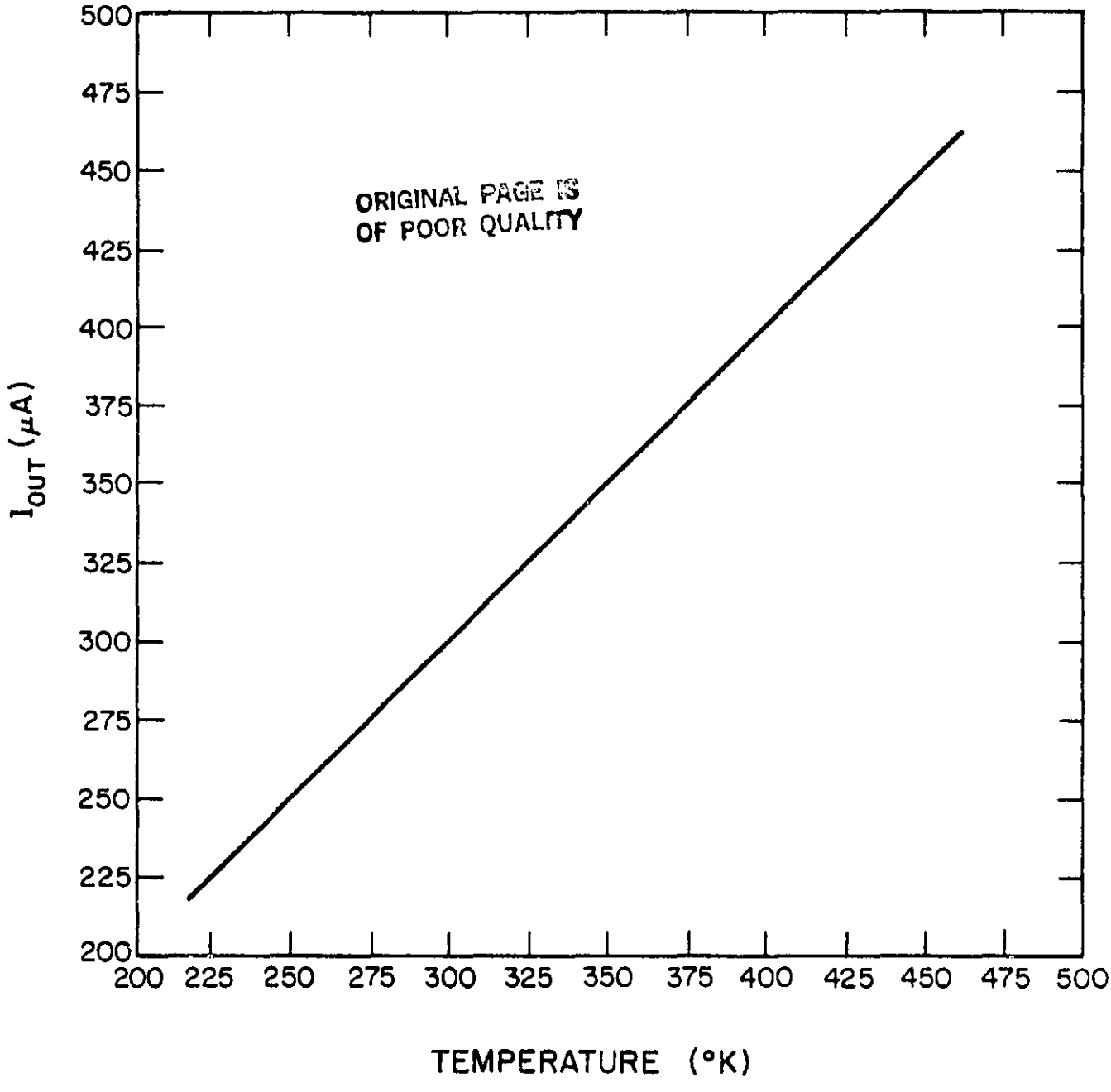

Figure 3.6 Plot of the output current versus temperature for the Analog Device AD590: two-terminal temperature transducer.

large base-to-emitter reverse voltage. A 1 kΩ resistor is connected to the base to limit the base current to 10.84 mA. The driving transistor is a 2N2102 NPN silicon transistor with a maximum collector current of 1.0 A and a minimum β of 10. The transistor used had a β of approximately 24 giving a maximum collector current of 260 mA. The maximum power dissipated in resistor R131 is 6.76 W, slightly greater than the rated 5 watts. Although this created no problems in the prototype circuit after several hours of testing, it is recommended that the heater resistor be replaced by a 10 W resistor in the flight instrument.

3.2.5 *Gain amplifier.* The third part of the magnitude detector is a gain amplifier. A National Semiconductor LM201 operational amplifier connected in the inverting mode is used to provide the necessary gain. With R112 and R113 (Figure 3.4) set equal to 10 kΩ and 100 kΩ, respectively, the gain of the amplifier is equal to 10. An additional resistor, R116, is placed in the output line to protect the operational amplifier from short circuits. The overall performance of the magnitude detector is presented later (section 3.6). Figure 3.7 is a picture of the magnitude detector as implemented on a printed circuit card.

3.3 *Phase Detector*

3.3.1 *Introduction.* The phase detector circuit for the electric field meter consists of three main parts: a zero crossing detector, an optical switch and an asynchronous sequential network, as indicated in Figure 3.8. The unit is designed to accept ac signals in the voltage range of 2 mV to 18 V (peak), and produce an output voltage of 0 V or 5 V in the form of a train of pulses containing the phase information. It should be noted that the input signal range of the phase detector circuit is similar to that of the magnitude detector circuits: both circuits are useful over four decades

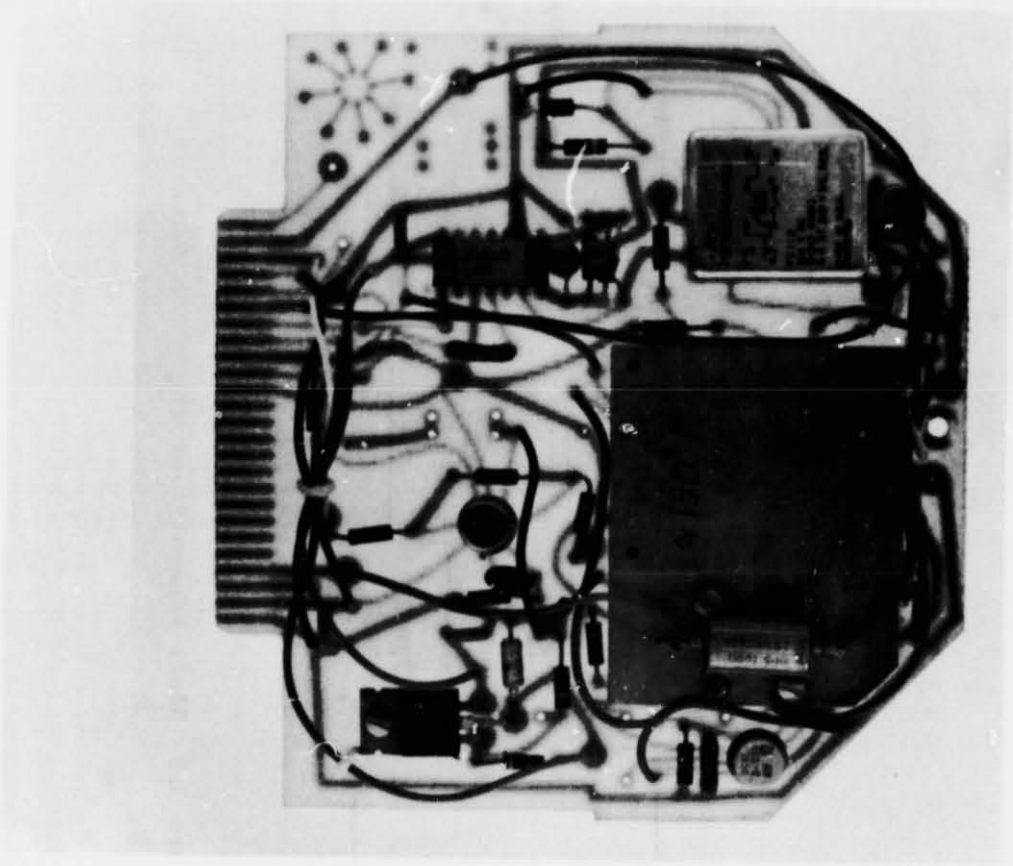

Figure 3.7 Magnitude detector and temperature regulated cavity implemented on a printed circuit card.

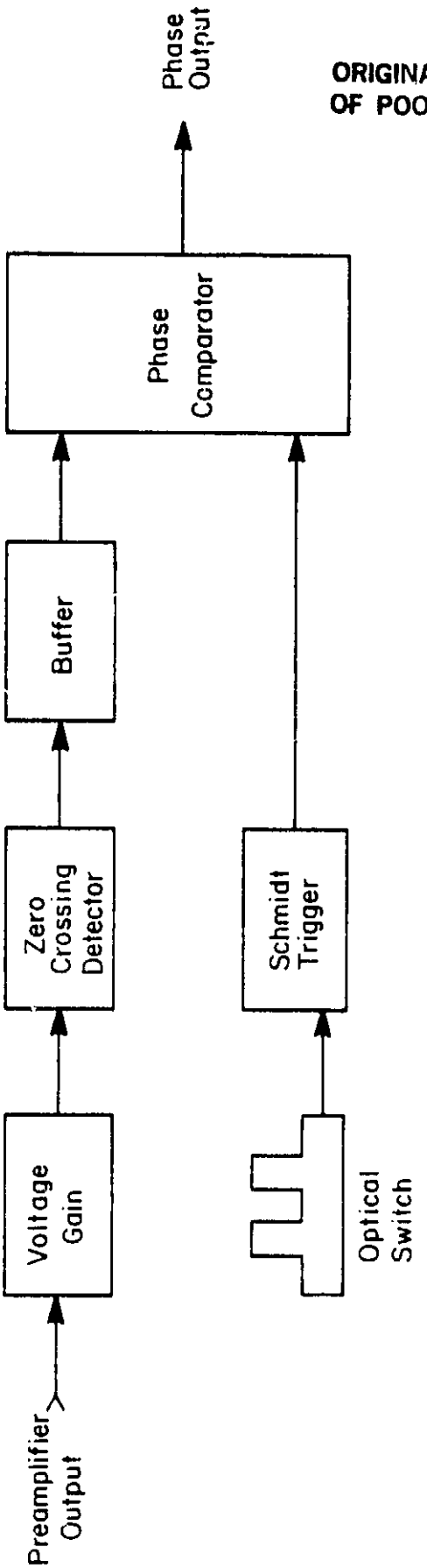

Figure 3.8 Block schematic of the phase detector.

of ac input voltages. In addition, both units can accept any periodic ac input signal; thus, design changes in the preamplifier or even the rotor-stator combination present no difficulties.

3.3.2 *Zero crossing detector.* The schematic for the zero-crossing-detector circuit is shown in Figure 3.9. The first operational amplifier is connected in the non-inverting mode and set to have a gain of 100. This gain essentially sets the hysteresis value of the following LM239. Using the recommended circuit presented in the National Semiconductor Linear Data-book, the LM239 circuit has a hysteresis value of ±0.2 V; i.e., once the unit is LOW it takes a V_{IN} greater than +0.2 V to change it to HIGH. With the gain of the LM201, this ±0.2 V is reduced to ±2 mV.

In testing it was found that the LM201 produced a slight dc offset measured at the output. To alleviate this problem, capacitor C109 is used to block any dc component, while resistor R120 is used to bleed off any dc voltage on the capacitor (refer to Figure 3.9). The comparator A9 (a 741 op amp) is used to buffer the LM239 from the rest of the circuit. In order to make the signal compatible with TTL gates, a 5.1 volt zener diode is used in the output circuit of the 741.

From Figure 3.9 one sees that the output is labeled TP8 STOP. The leading edge of this signal provides one of the two inputs needed by the phase comparator.

3.3.3 *Reference signal.* A chopper blade on the motor shaft and a Monsanto MCA81 optical switch produce the reference signal needed by the phase comparator. The output transistor of the MCA81 is ON when the infrared light beam is uninterrupted, Figure 3.10. In this state, the transistor sinks current from a Schmidt trigger NAND gate (SN74132) causing its output to go to HIGH. Similarly, when the chopper blade blocks the light beam, the

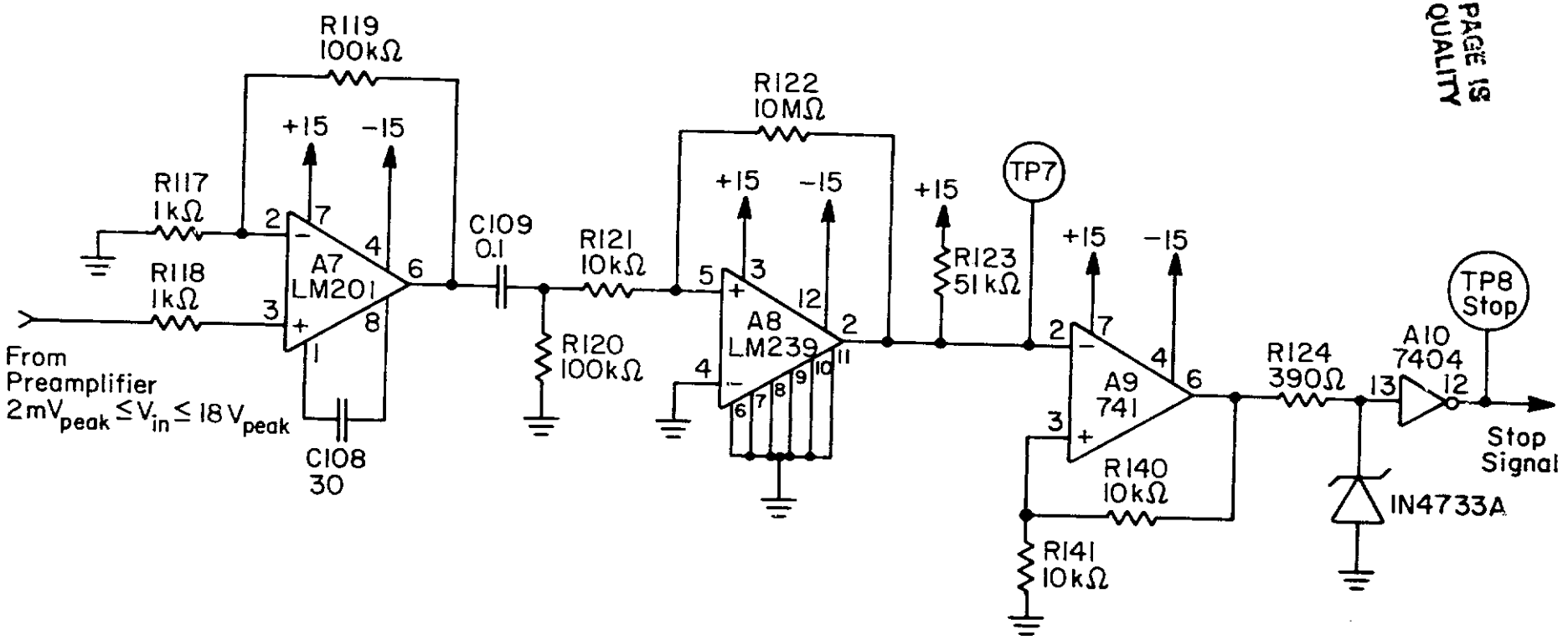

Figure 3.9 Circuit of the zero-crossing detector used in the phase detector.

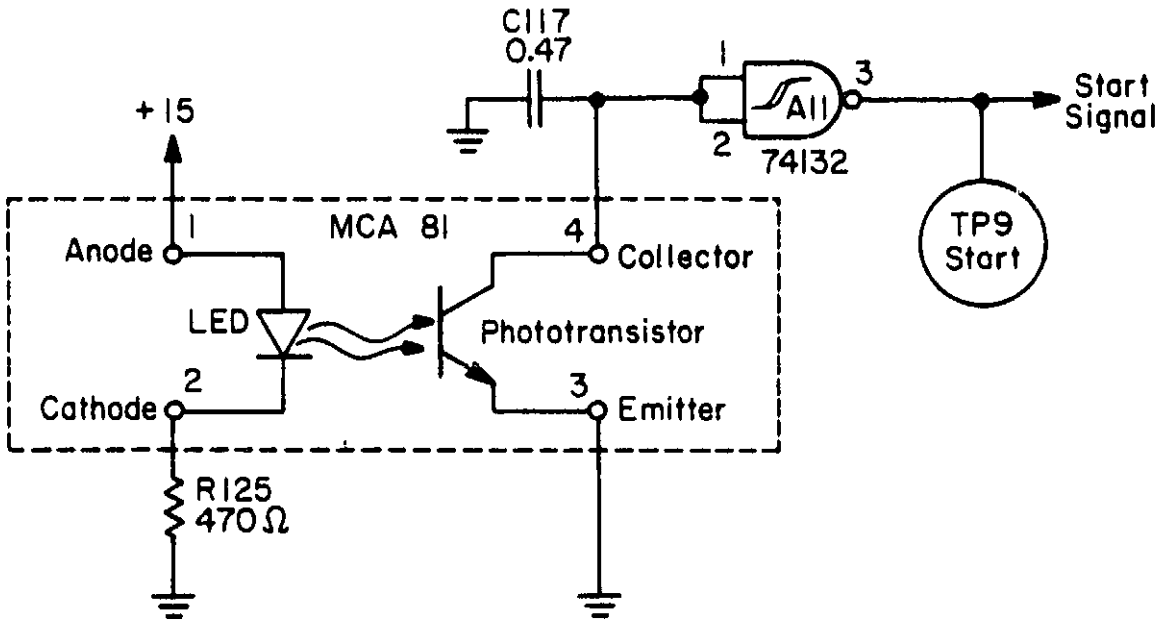

Figure 3.10 Circuit used to generate the phase reference START signal. The optical switch is the Monsanto MCA81.

output transistor of the optical switch is OFF and the output of the Schmidt trigger NAND gate goes LOW. Since the switching time of the MCA81 is 200 μs, the unit can be operated safely at 100 Hz. Capacitor C117 is necessary to supress noise spikes which may cause the circuit to operate incorrectly.

3.3.4 *Phase comparator.* Using the START signal generated by the phase reference and the STOP signal generated by the transducer the phase difference is obtained in an asynchronous sequential network. The logic of the phase comparator will now be described.

The 0-to-1 transition of the START signal sets the output of an asynchronous sequential network HIGH. The 0-to-1 transition of the STOP signal sets the output of the sequential network LOW. Since the START signal has a 0-to-1 transition every 360°, the time that the output is HIGH in relation to the total time between consecutive 0-to-1 transitions of the output determines the phase angle of the input wave relative to the reference. Furthermore the time between consecutive leading edges of the sequential network's output gives a measurement on the operating speed of the motor. For the operating frequency of 100 Hz the time between the leading edges is 10 ms.

Another point of concern is the sign of the input sinusoid. Arbitrarily choosing 0° to correspond to a positive electric field producing all displacement current and no conduction current, one can expect the following phase angles for conditions when conduction current is significant:

$$0° \leq \phi \leq 90° \text{ for positive fields}$$

$$180° \leq \phi \leq 270° \text{ for negative fields.}$$

These follow from the considerations of section 2.1 and are illustrated in Figure 3.11. One can see that for a positive electric field producing only a displacement current the resultant phase angle ϕ is 0°. Moreover, for a

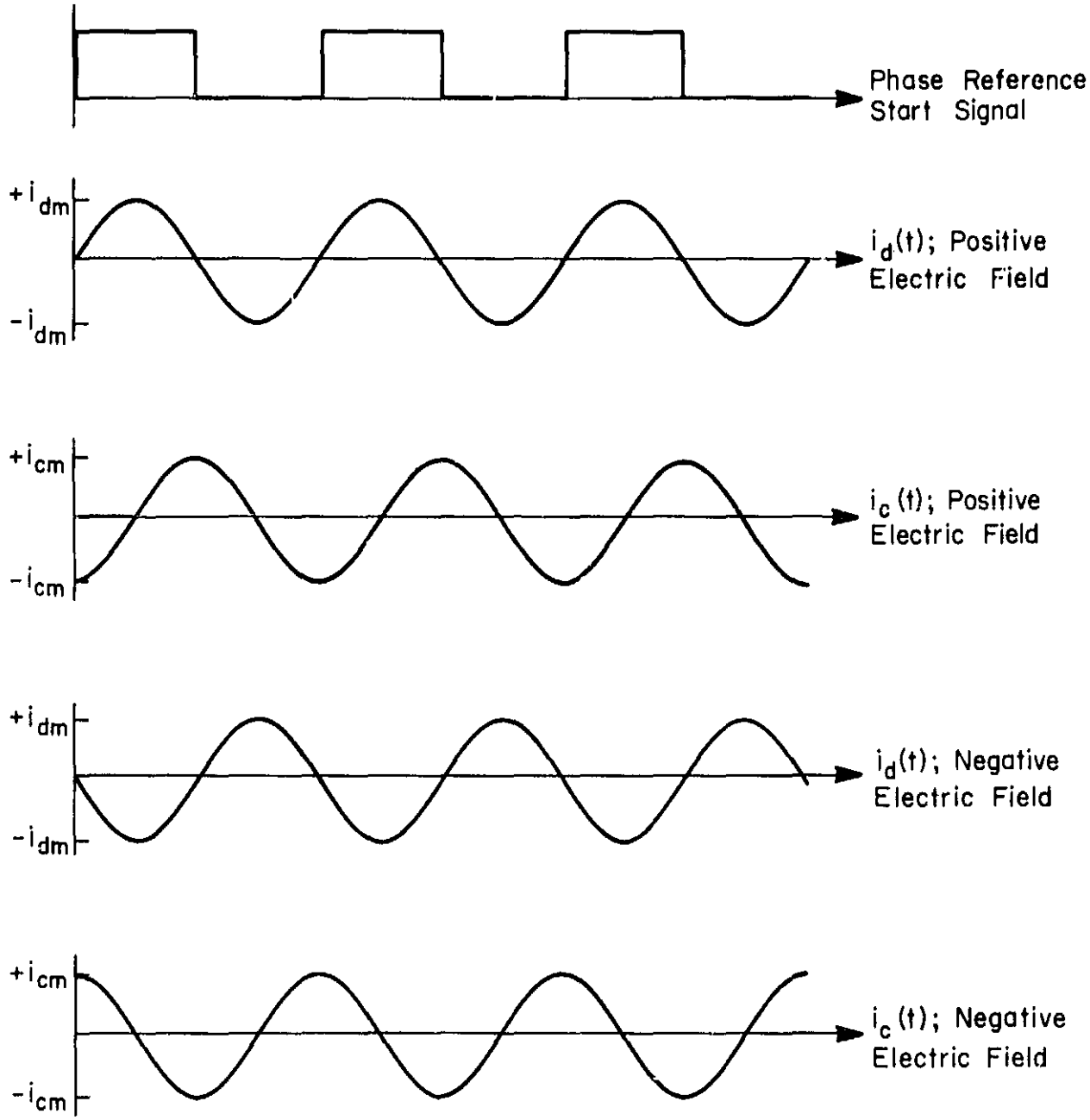

Figure 3.11 Relative phases of displacement current and conduction current for positive and negative electric fields compared with the phase reference START signal.

positive electric producing only a conduction current the phase angle is 90°. In like manner, for negative electric fields ϕ is equal to 180° for displacement current only, and to 270° for conduction current only. When both conduction current and displacement current are present it is evident that for positive electric fields $0° \leq \phi \leq 90°$ and for negative field $18° \leq \phi \leq 270°$.

An asynchronous sequential network has been designed to indicate the phase of the input since no commercially available IC phase comparator was found to perform the desired function. At first it was thought that a four-quadrant detector would work, but after further investigation it was found that the unit responded incorrectly to certain input patterns.

In designing the sequential network it was found that six states are necessary even though two of the six are dummy states. The meaning of these states (labeled A, B, C, D, E, and F) are given in Table 3.3. The two dummy states, E and F, are necessary to prevent racing. For example (refer to Figure 3.12), if one is in state A with inputs (START, STOP) equal to (0,0) and the inputs change simultaneously to (1,1) the sequential network could possibly view the inputs momentarily as (0,1) in which case the network would race through states C and E and then stop in state B instead of reaching the desired state D.

Using the state assignments shown in Table 3.3, the network was designed using S-R flip-flops, as discussed by *Muroga* [1979]. Table 3.4 shows the desired state-output table which corresponds to the state transition diagram (Figure 3.12). Table 3.5 is the input-output relationship of an S-R flip-flop which is used along with the state-output table to form the desired excitation and output tables (Tables 3.6 and 3.7).

Since $\overline{S}$-$\overline{R}$ flip-flops were readily available, the network was designed for S-R flip-flops and then the logic functions for S and R were complemented.

Table 3.3 State assignments for the phase-comparator sequential network.

A:	Looking for leading edge of START; START low	(000)
B:	Looking for leading edge of START; START high	(001)
C:	Looking for leading edge of STOP; STOP low	(100)
D:	Looking for leading edge of STOP; STOP high	(110)
E:	Dummy state to prevent racing	(101)
F:	Dummy state to prevent racing	(010)

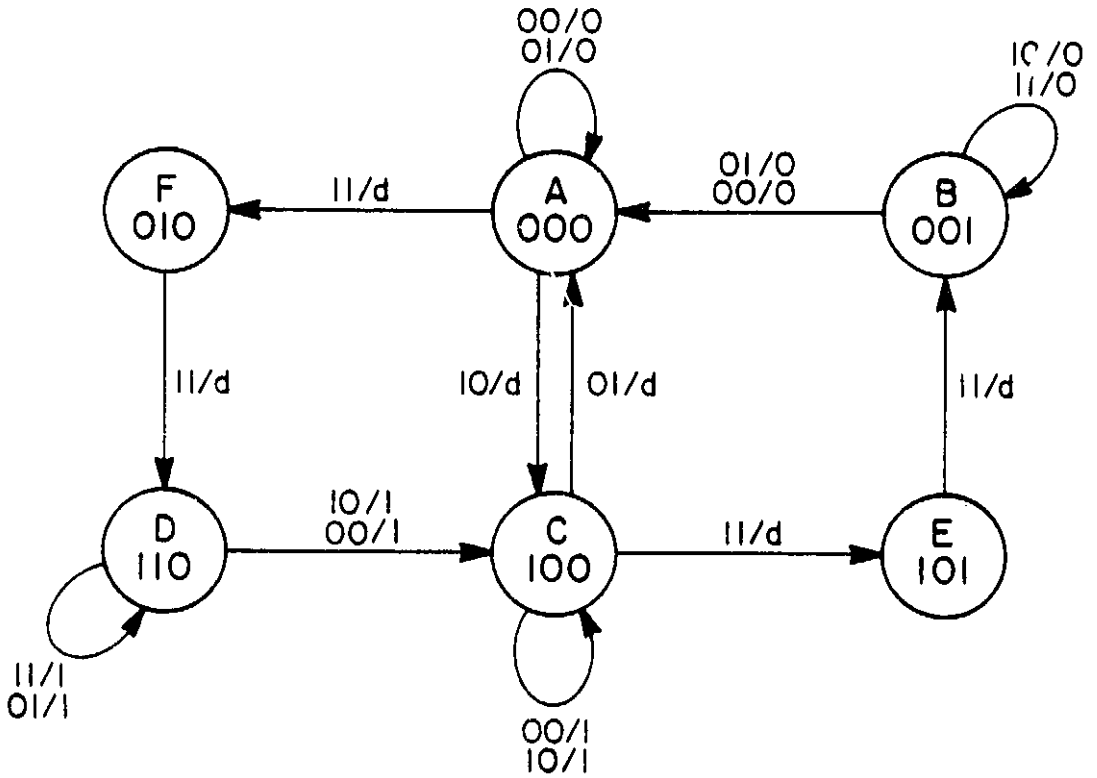

Figure 3.12 State transition/output diagram of the phase comparator used in this phase detector. The significance of the six states is given in Table 3.3.

Table 3.4 State-output table for the phase comparator asynchronous sequential network.

(y_1, y_2, y_3)	(START/STOP) 00	01	11	10
A ∿ 000	000/0	000/0	010/d	110/d
B ∿ 001	000/0	000/0	001/0	001/0
C ∿ 100	100/1	000/d	101/d	100/1
D ∿ 110	100/1	110/1	110/1	100/1
E ∿ 101	001/d	001/d	001/d	001/d
F ∿ 010	110/d	110/d	110/d	110/d

d = don't care

Table 3.5 Input-output relationship of an S-R flip-flop.

INPUT		OUTPUT	
y	y	S	R
0	0	0	d
0	1	1	0
1	0	0	1
1	1	d	0

d = don't care.

Table 3.6 Excitation tables for S-R flip-flops used in the phase comparator.

(y_1, y_2, y_3)		(START, STOP) 00	01	11	10
A	000	0	0	0	1
B	001	0	0	0	0
F	010	1	1	1	1
-	011	d	d	d	d
C	100	d	0	d	d
E	101	0	0	0	0
D	110	d	d	d	d
-	111	d	d	d	d

$S_1 = y_2 \vee \overline{y_3}\ \text{START}\ \overline{\text{STOP}}$

(y_1, y_2, y_3)		(START, STOP) 00	01	11	10
A	000	d	d	d	0
B	001	d	d	d	d
F	010	0	0	0	0
-	011	d	d	d	d
C	100	0	1	0	0
E	101	1	1	1	1
D	110	0	0	0	0
-	111	d	d	d	d

$R_1 = y_3 \vee \overline{y_2}\ \overline{\text{START}}\ \text{STOP}$

(y_1, y_2, y_3)		(START, STOP) 00	01	11	10
A	000	0	0	1	0
B	001	0	0	0	0
F	010	d	d	d	d
-	011	d	d	d	d
C	100	0	0	0	0
E	101	0	0	0	0
D	110	0	d	d	0
-	111	d	d	d	d

$S_2 = \overline{y_1}\overline{y_3}\ \text{START}\ \text{STOP}$

(y_1, y_2, y_3)		(START, STOP) 00	01	11	10
A	000	d	d	0	d
B	001	d	d	d	d
F	010	0	0	0	0
-	011	d	d	d	d
C	100	d	d	d	d
E	101	d	d	d	d
D	110	1	0	0	1
-	111	d	d	d	d

$R_2 = y_1\ \overline{\text{STOP}}$

(y_1, y_2, y_3)		(START, STOP) 00	01	11	10
A	000	0	0	0	0
B	001	0	0	d	d
F	010	0	0	0	0
-	011	d	d	d	d
C	100	0	0	1	0
E	101	d	d	d	d
D	110	0	0	0	0
-	111	d	d	d	d

$S_3 = y_1\overline{y_2}\ \text{START}\ \text{STOP}$

(y_1, y_2, y_3)		(START, STOP) 00	01	11	10
A	000	d	d	d	d
B	001	1	1	0	0
F	010	d	d	d	d
-	011	d	d	d	d
C	100	d	d	0	d
E	101	0	0	0	0
D	110	d	d	d	d
-	111	d	d	d	d

$R_3 = \overline{y_1}\ \overline{\text{START}}$

Table 3.7 Output table of the asynchronous sequential network used in the phase comparator.

(y_1, y_2, y_3)		(START, STOP)			
		00	01	11	10
A	000	0	0	d	d
B	001	0	0	0	0
F	010	d	d	d	d
-	011	d	d	d	d
C	100	1	d	d	1
E	101	d	d	d	d
D	110	1	1	1	1
-	111	d	d	d	d

$Z = y_1$

The logic functions for the three $\overline{S}$-$\overline{R}$ flip-flops are shown in Table 3.8.

Figure 3.13 shows the schematic of the resulting asynchronous sequential network as designed using NAND, NOR and NOT gates. Figure 3.14 is a picture of the phase detector as constructed on a printed circuit card.

3.4 *Digital Phase Display*

The digital phase display is designed to accept the output from the phase detector circuit and to display the phase angle. The phase angle, ϕ, is defined in terms of the ratio of the time the phase output remains HIGH to the time between consecutive leading edges of the phase output. Referring to Figure 3.15

$$\phi = (t_{high}/t_{total}) \times 360° \qquad (3.7)$$

The nominal value of t_{total} for the electric field meter is 10 ms. From equation (3.7) it is seen that t_{high} is 27.78 μs per degree of phase difference so that t_{high} divided by 27.78 μs yields the phase angle ϕ in degrees. In order to implement this, a 555 timer running in the asynchronous mode at 36 kHz (a period of 27.78 μsec) is ANDed with the phase output. A SN74143 is used to count the number of 555 pulses passed by the AND gate, the number of pulses being equal to the phase angle ϕ. The schematic for the digital phase display circuit is illustrated in Figure 3.16. A trim potentiometer (R135) is used to fine tune the 555 to 36 kHz. A picture of the finished circuit is shown in Figure 3.17.

The timing signals are shown in Figure 3.18. It will be seen that the phase display is updated every 20 ms. It should also be noted that the digital phase display is not part of the rocket payload. The display is to aid in the testing and calibration of the completed field meter.

Table 3.8 Logic functions for the $\overline{S}$-$\overline{R}$ inputs to the flip-flops used in the phase comparator circuit.

$$\overline{S_1} = y_2 V (y_3 V (START \cdot \overline{STOP}))$$

$$\overline{R_1} = y_3 V (y_2 V (\overline{START} \cdot STOP))$$

$$\overline{S_2} = (\overline{y_1 V y_3}) \cdot (\overline{START V STOP})$$

$$\overline{R_2} = \overline{y_1 \cdot \overline{STOP}}$$

$$\overline{S_3} = (\overline{y_1} V y_2) \cdot (\overline{START V STOP})$$

$$\overline{R_3} = \overline{\overline{y_1} \cdot \overline{START}}$$

ϕ output = y_1

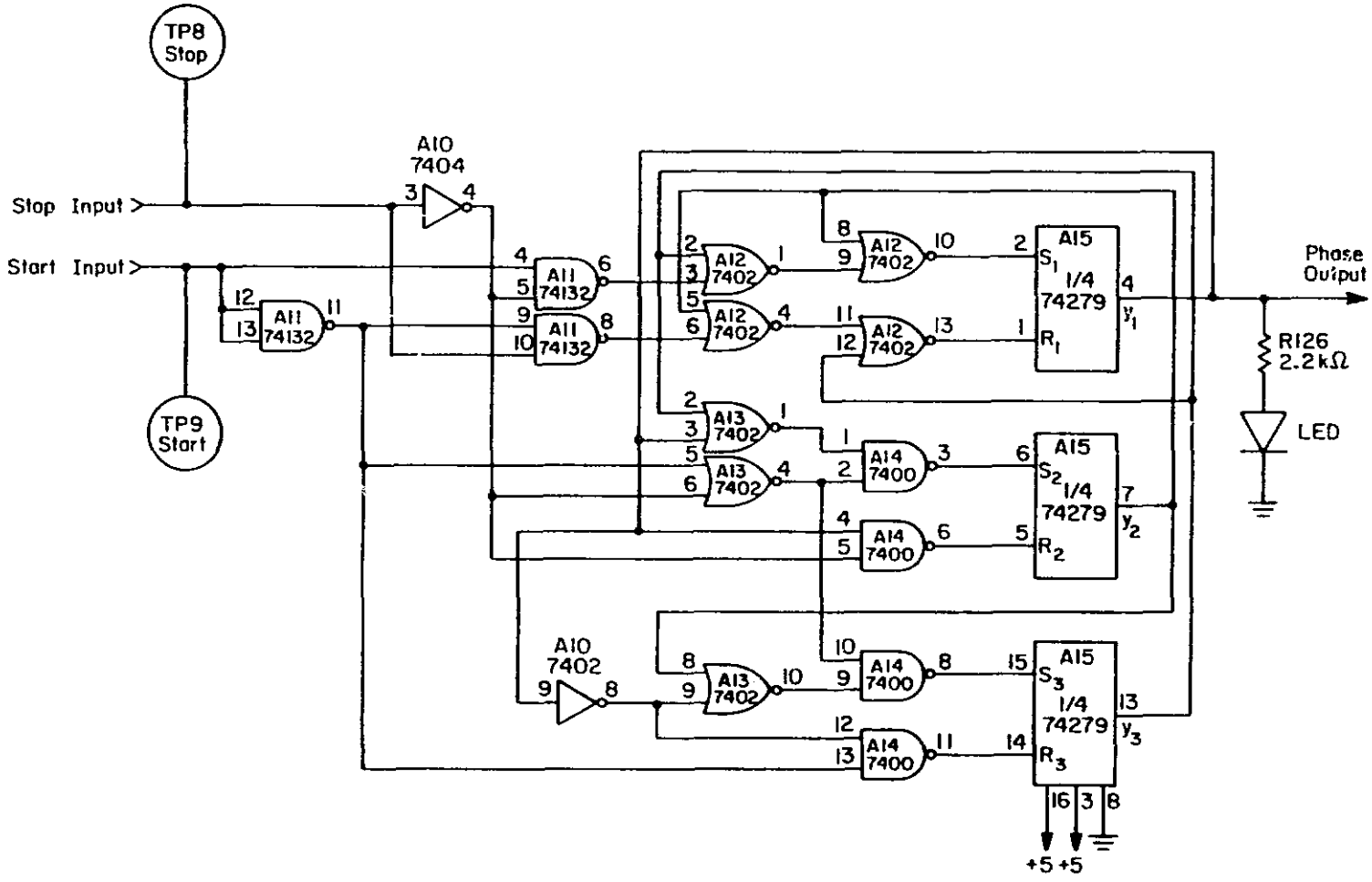

Figure 3.13 Circuit of the phase comparator used in the phase detector. The phase comparator is a six state asynchronous sequential network.

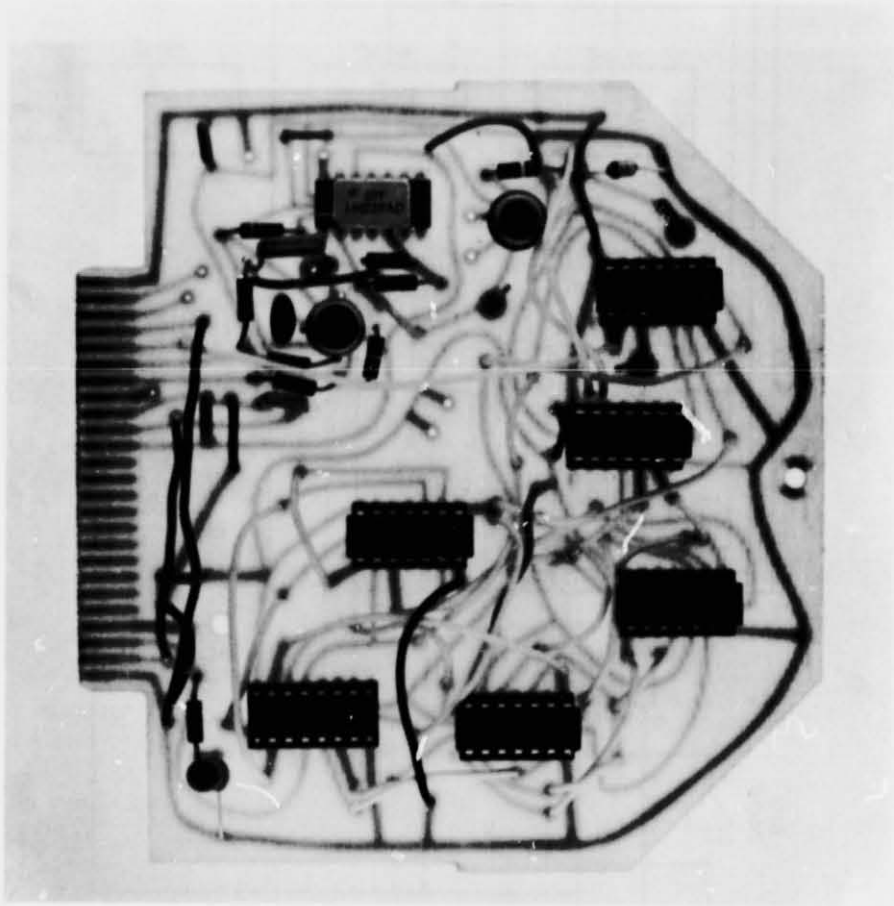

Figure 3.14 The phase detector circuit as implemented on a printed circuit card.

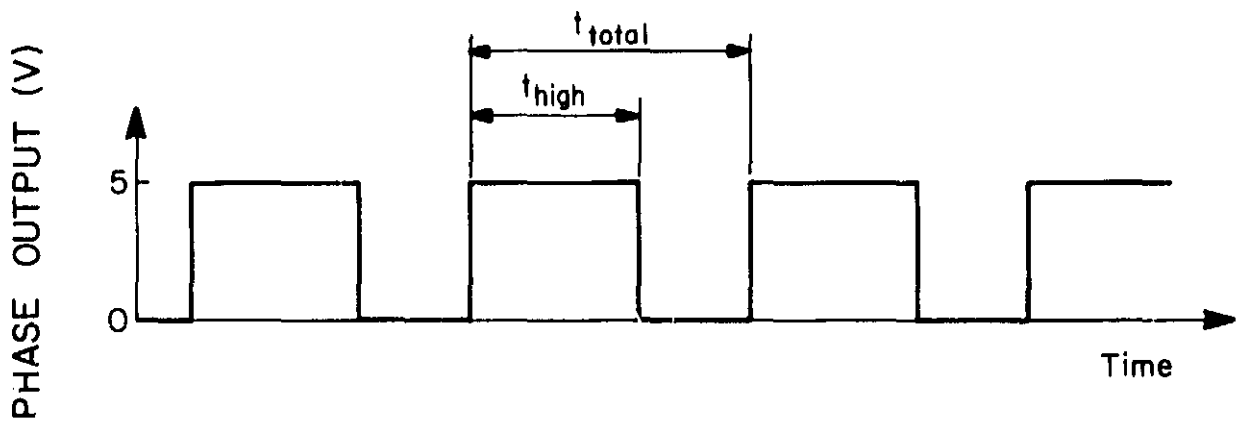

Figure 3.15 Typical phase detector output signal showing the relationship between t_{high} and t_{total} as referred to in equation (3.7). The time between consecutive leading edges of this signal gives a measurement on the period of the input sinusoid and, hence of the motor speed.

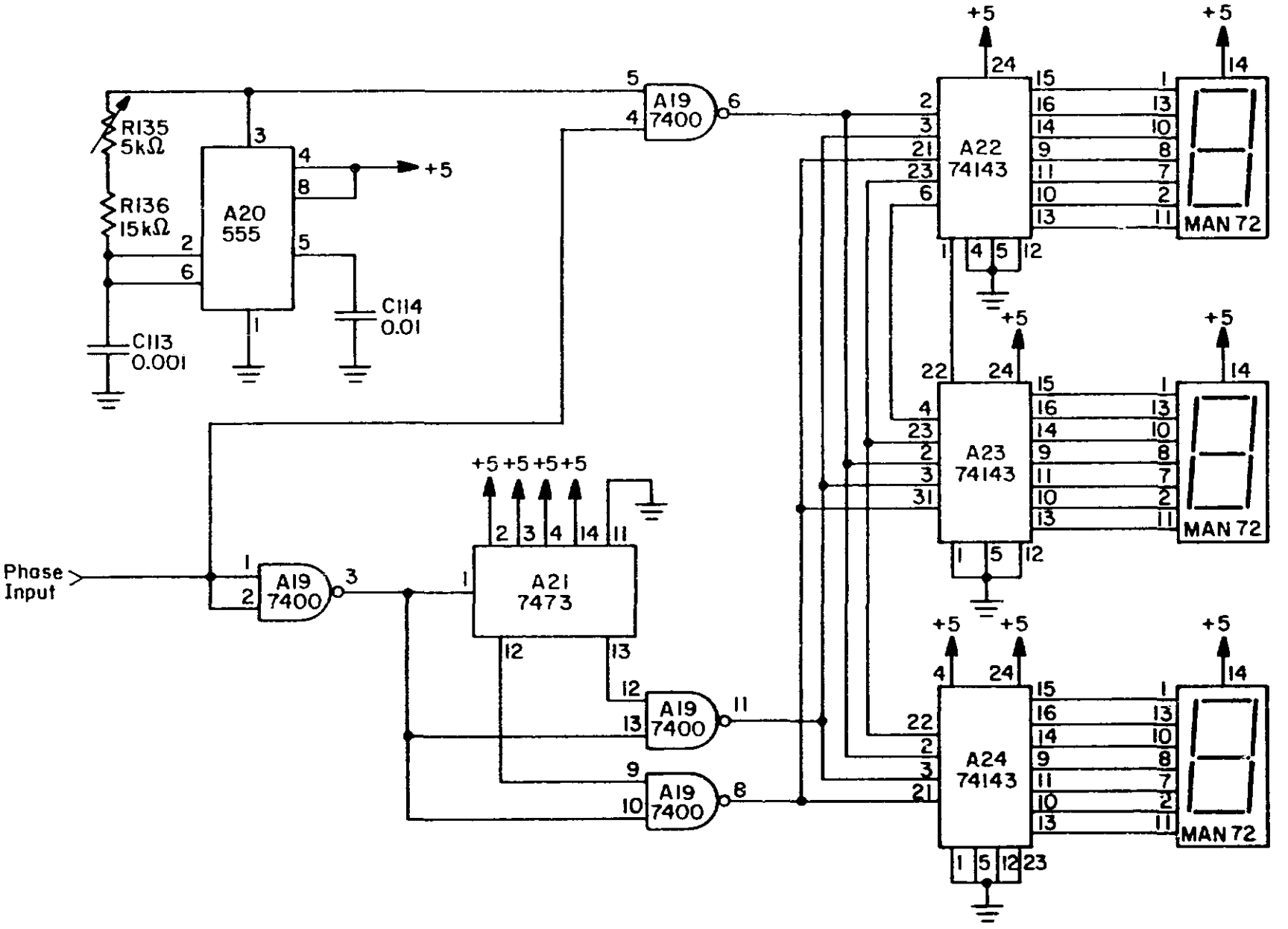

Figure 3.16 Circuit of the digital phase display.

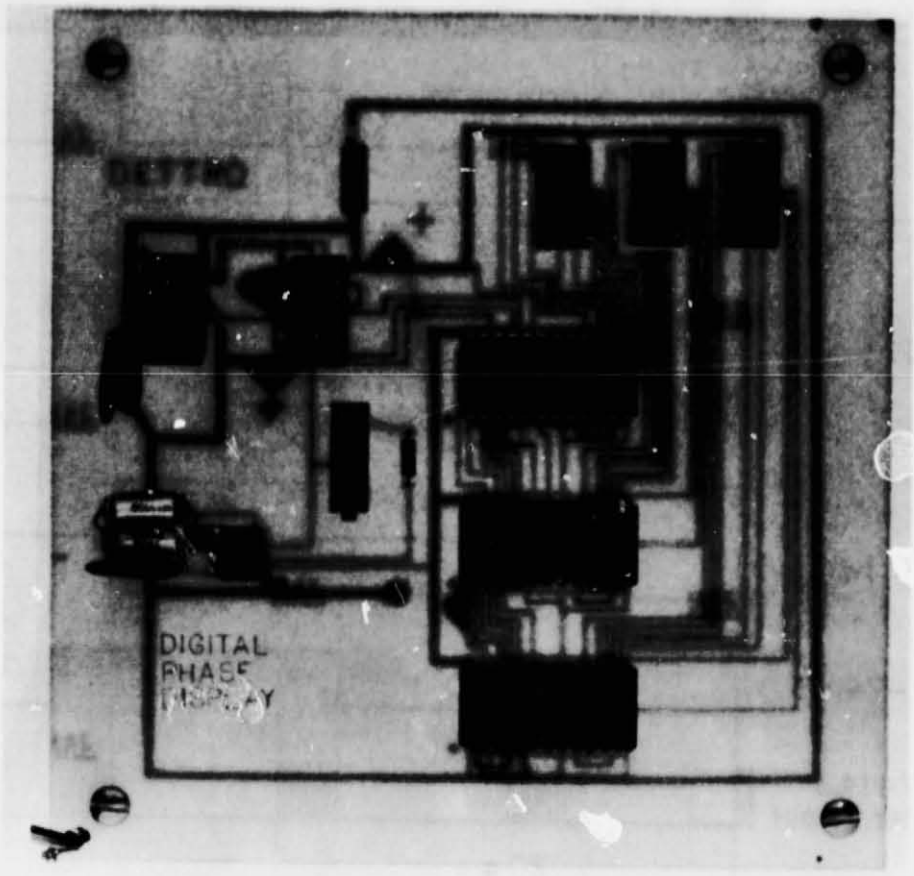

Figure 3.17 The digital phase display as implemented on a printed circuit card.

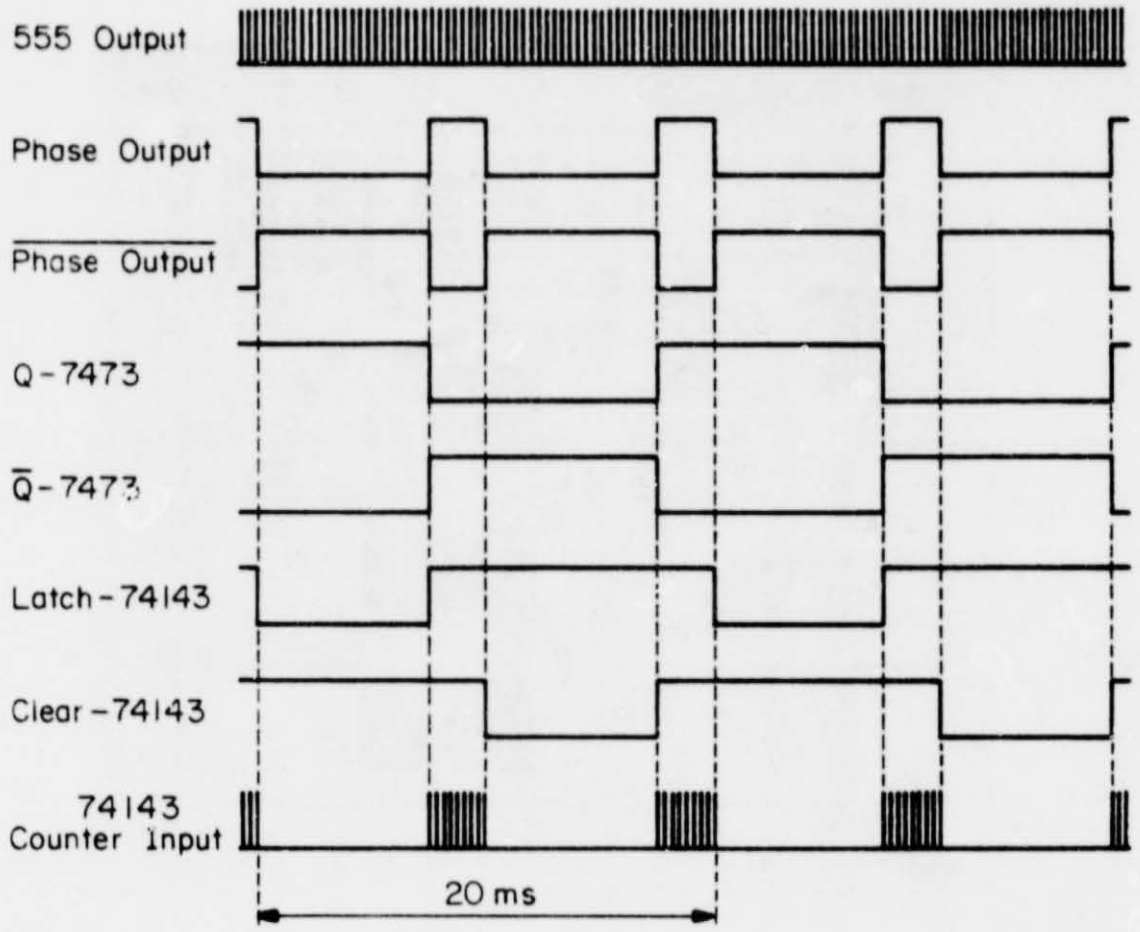

Figure 3.18 Timing diagram for the digital phase display circuit. The 555 IC timer output pulses are drawn as a low frequency for added clarity. The display is updated every 20 ms as denoted by the LATCH pulses.

3.5 *Motor Voltage Control*

The dc motor used in the system requires a separate voltage regulator in order to achieve the desired operating speed. Figure 3.19 shows this voltage regulator: an LM317 adjustable positive regulator. A 22 Ω (5 W) resistor is placed on the input of the regulator in order to reduce the power dissipation in the regulator. The motor speed is controlled by R132, chosen to be 10 kΩ. This produces the output voltage of +5.5 V needed to drive the motor at 1500 rpm. If a different motor is substituted for the motor currently in the system, the necessary driving voltage is available from this regulator by adjusting R132.

3.6 *Circuit Test and Simulation*

Testing the electronic circuits is most easily accomplished by use of the nine test points shown earlier in Figures 3.2, 3.4, 3.5, 3.9, 3.10, 3.13, and 3.16. With reference to these test points, a signal applied at a test point implies that the circuit preceding that test point is disconnected.

3.6.1 *Preamplifier.* Test point 1, Figure 3.2, is a point at which the output of the picoampere-to-voltage converter can safely be measured. By applying a triangular waveform through a 10 pF capacitor to the input of the preamplifier one sees the response of the circuit to a square-wave current input (a displacement current). At an input frequency of 100 Hz

$$I_{IN} = C\frac{dV}{dt} = 2 \times 10^{-9} V_{p-p} \tag{3.8}$$

The time constant of the converter, determined by R101 and C101, can be measured at test point 1. This can conveniently be done at the same time that the gain of the converter is measured. The time constant is measured to be 1 ms with the R101 - C101 feedback elements yielding a cutoff frequency of 160 Hz. The gain of the current-to-voltage converter is found to be close to

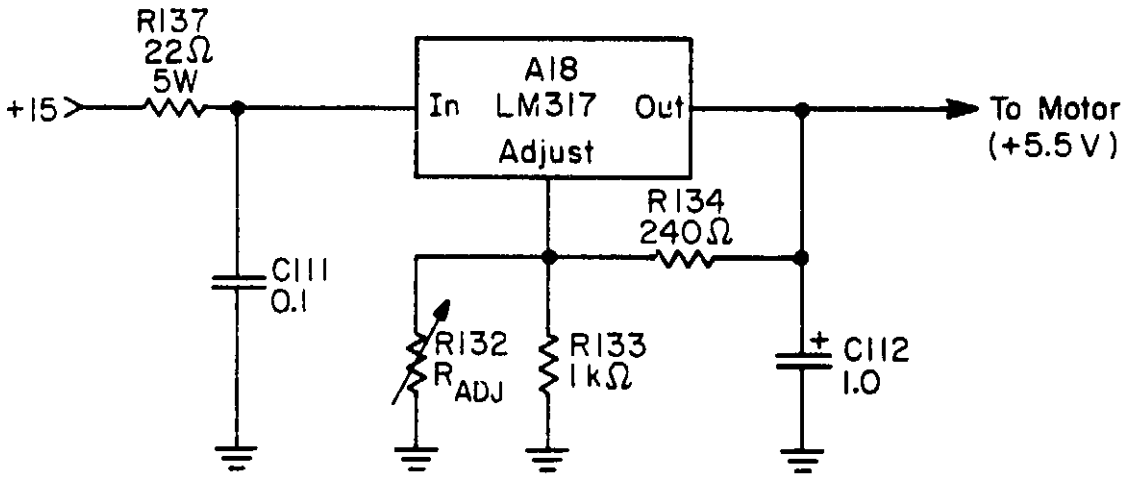

Figure 3.19 Circuit of the voltage regulator used to supply the motor. R132 adjusts the output voltage and therefore the motor speed.

1 mV/pA, corresponding to the 10^9 Ω feedback resistor.

Applying a signal applied at test point 1, the output of the gain amplifier is measured at test point 2. Using a 100 Hz sine-wave input, the gain is found to be 5.2.

Figure 3.20 shows the input current versus the output voltage for the preamplifier. From these data it is evident that the preamplifier has a gain of 5.49 mV/pA. Moreover the system will operate for input currents in the range of 4 pA to 2.24 nA.

3.6.2 *Magnitude detector.* Test points 3 and 4 in Figure 3.4 are used to evaluate the performance of this circuit. As has already been noted (in section 3.2.2) the AD536 proved to be very accurate and therefore no further calibrations were necessary.

The logarithmic amplifier was tested in a temperature-controlled oven from 70°F to 160°F. A dc signal was applied to test point 3 and the output voltage was then measured at test point 4. Figure 3.21 is a graphical view of these data at various temperatures. It should be noted that the accuracy of the temperature in Figure 3.21 is approximately ±2°F due to the coarse temperature scale readings obtainable from the thermometer on the temperature regulated oven. Figure 3.22 is a plot of the same logarithmic amplifier input voltages versus the magnitude detector output voltages. By using this graph, one is able to access the operating temperature of the logarithmic amplifier. This is done by applying a calibrate signal of +5.0 V at test point 3, Figure 3.4, and observing the magnitude output. This calibrate signal is applied by an electronic switch on the magnitude PC card. Figure 3.23 is a plot of the zener voltage, used to generate the +5.0 V signal, versus temperature. The

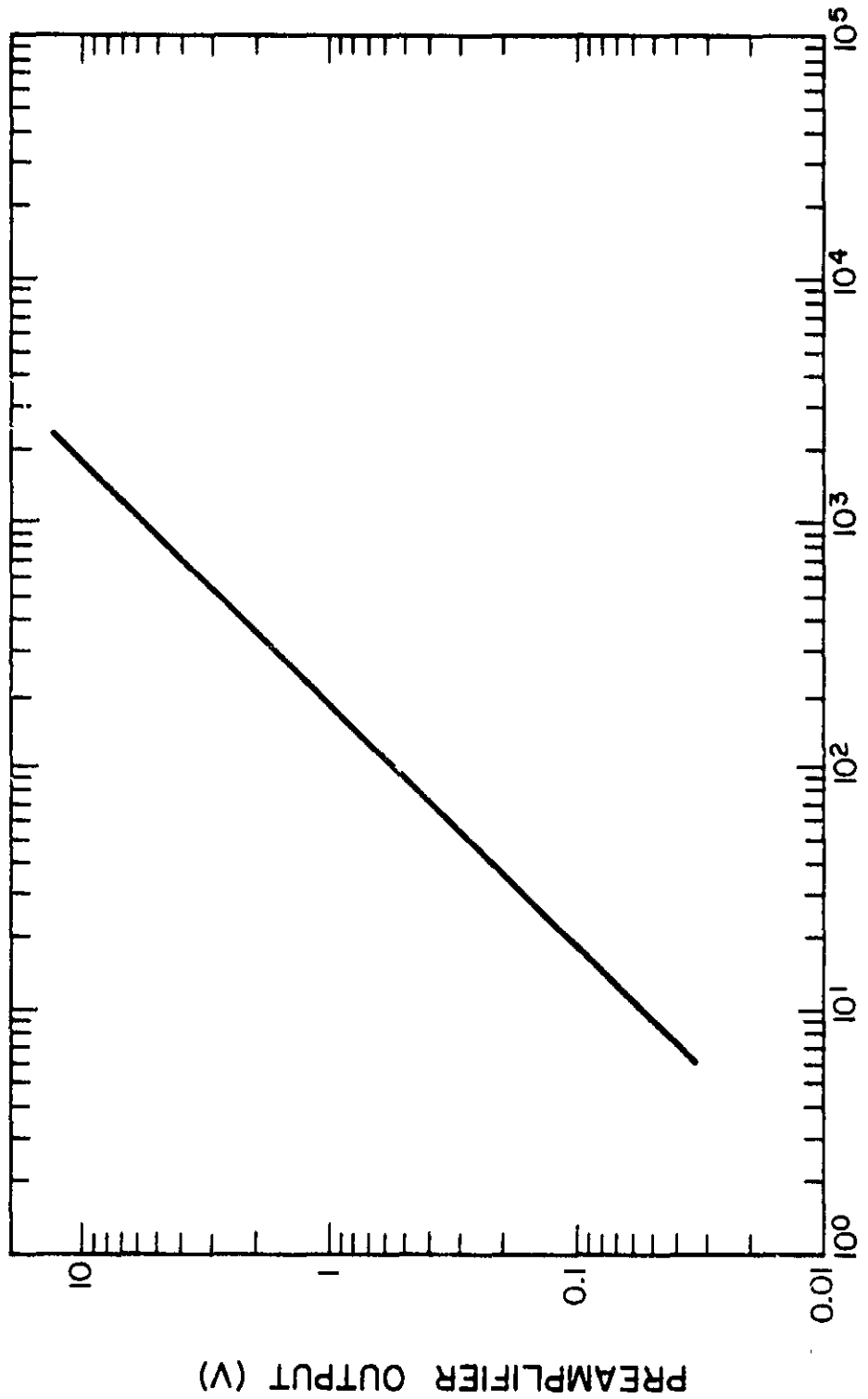

Figure 3.20 Input current versus output voltage for the preamplifier.

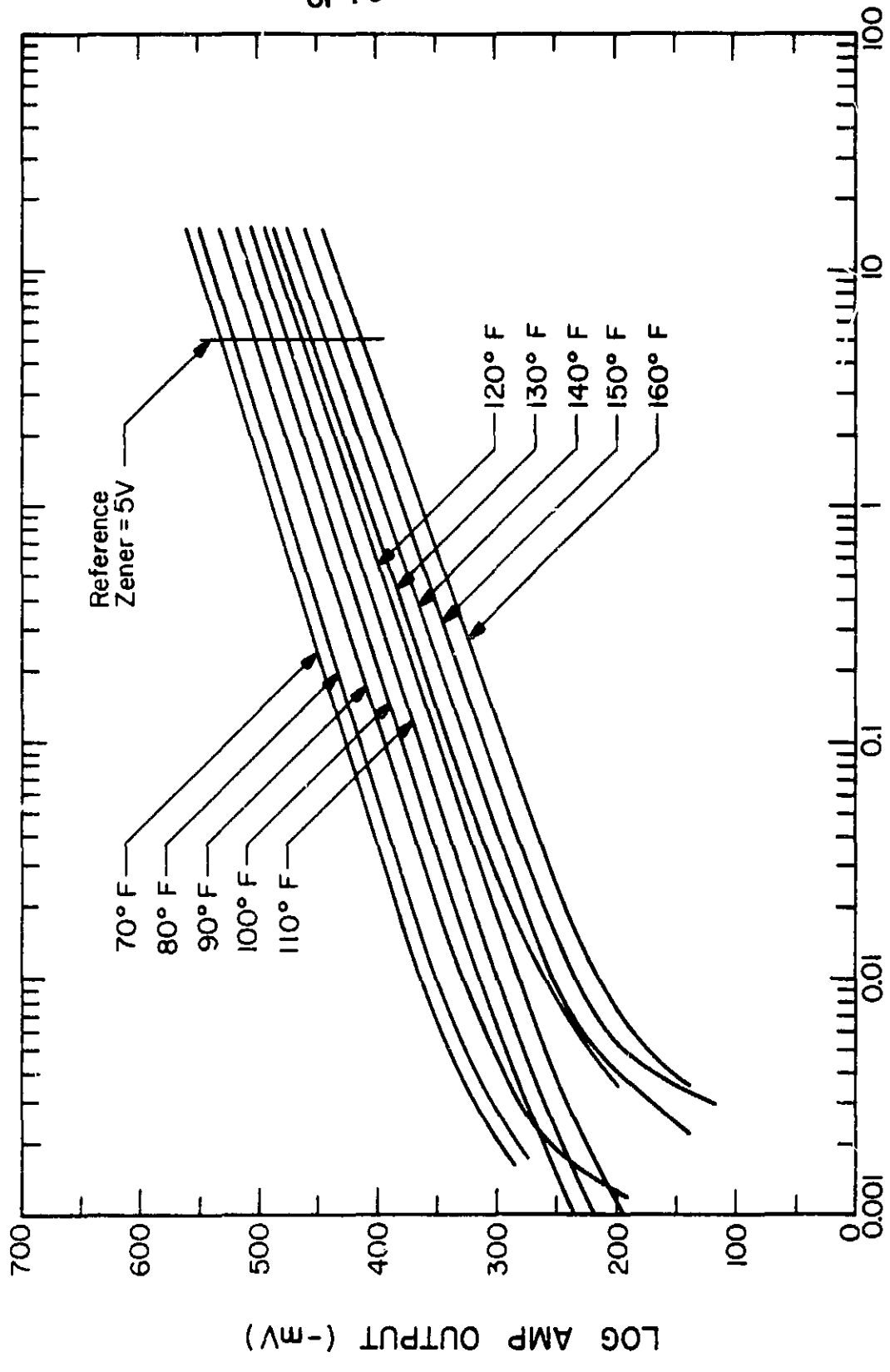

Figure 3.21 Temperature dependence of the output voltage of the logarithmic amplifier.

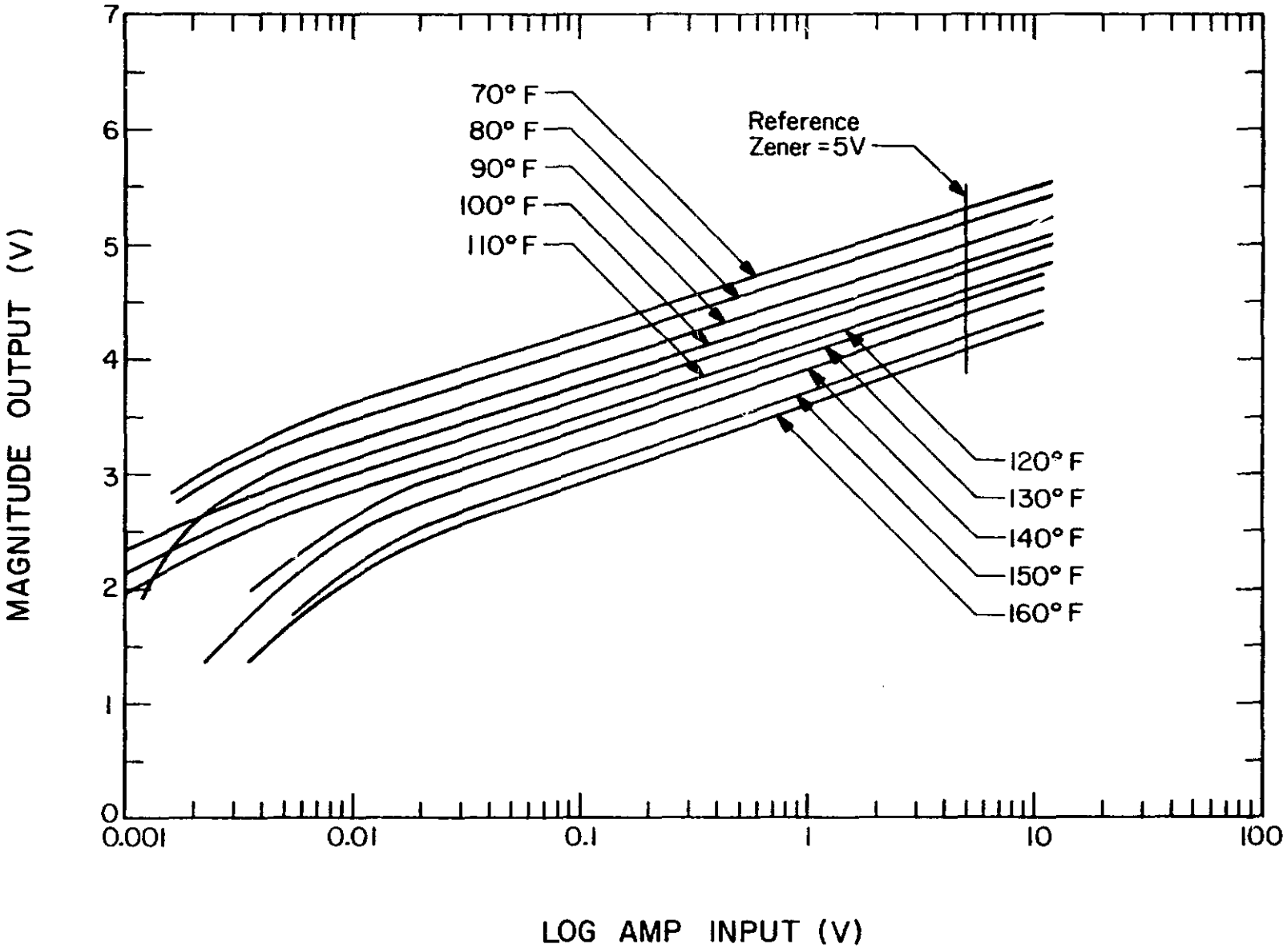

Figure 3.22 Temperature dependence of magnitude detector output voltage versus logarithmic amplifier input voltage.

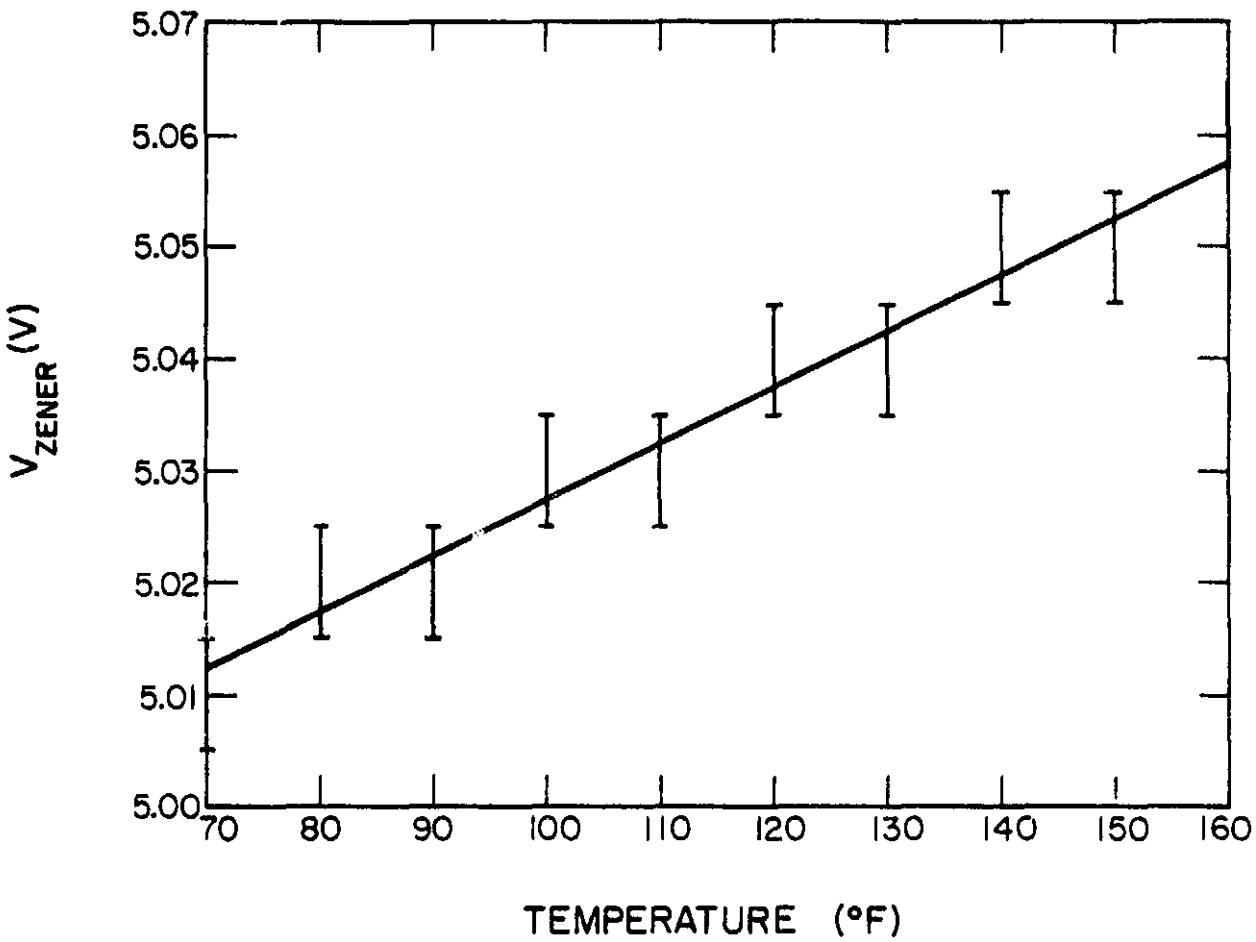

Figure 3.23 Plot of voltage of the zener diode (used as a +5.0 V reference signal) versus temperature.

zener voltage is relatively independent of temperature and can be assumed to be constant.

Once the logarithmic amplifier temperature curves are plotted, one is able to check the temperature of the temperature regulated cavity. With the logarithmic amplifier placed inside the cavity, the calibration procedure was repeated. First, a plot of the logarithmic amplifier input voltage versus output voltage was made, Figure 3.24. Figure 3.24 also shows a theoretical plot of the logarithmic amplifier input voltage versus output voltage predicted by equation (3.6). Comparing Figures 3.24 and 3.21 it is clear that the temperature regulated cavity held the temperature at 150°F. Second, a plot of the logarithmic amplifier input voltage versus magnitude detector output voltage was constructed, Figure 3.25. Finally, a 100 Hz sinusoid input was applied to the input of the magnitude detector and a plot of this input, in RMS volts, versus the magnitude detector output was made, Figure 3.26. The linearity of the system over four decades of input voltage is clearly seen.

Another check on the operating temperature is to measure the voltages at test points 5 and 6, Figure 3.5. One is able to obtain the actual temperature of the cavity by measuring the voltage at test point 6 and recalling that the AD590 has an output of 1 μV/°K. Taking this voltage and dividing it by R128 (10.3 kΩ) one can get the output current of the AD590. Dividing this current by 1 μV/°K one gets the cavity temperature in °K.

The theoretical operating temperature of the cavity is found by measuring the reference voltage at test point 5 and following the same procedure mentioned above. During testing, these voltages were both found to be 3.49 volts which corresponds to 340°K (150°F).

3.6.3 *Phase detector.* The front end of the phase detector circuit is a zero crossing detector with hysteresis. Applying a sinusoidal input to

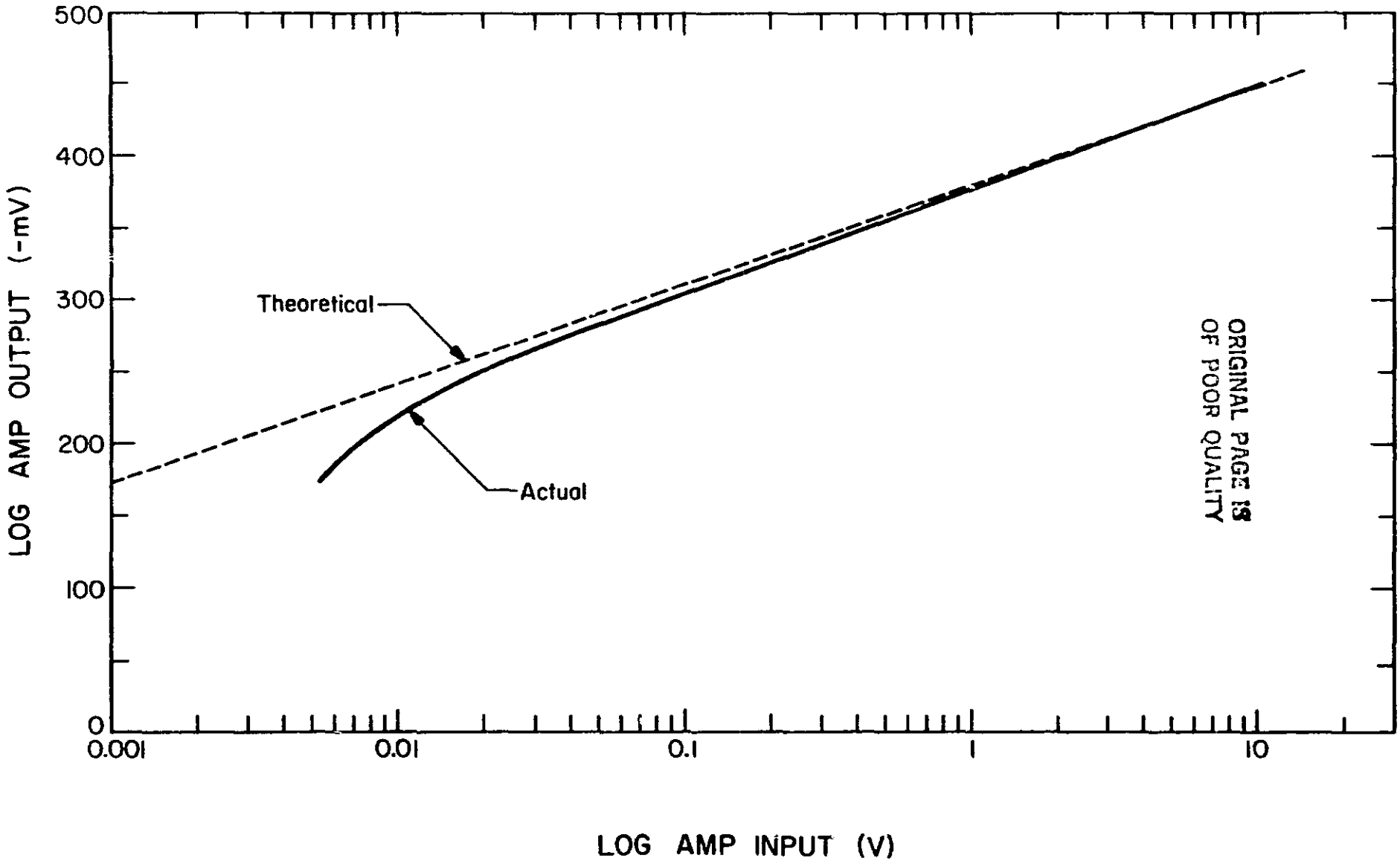

Figure 3.24 Theoretical and actual plots of logarithmic amplifier input voltages versus output voltages. Theoretical plot is predicted by equation (3.6).

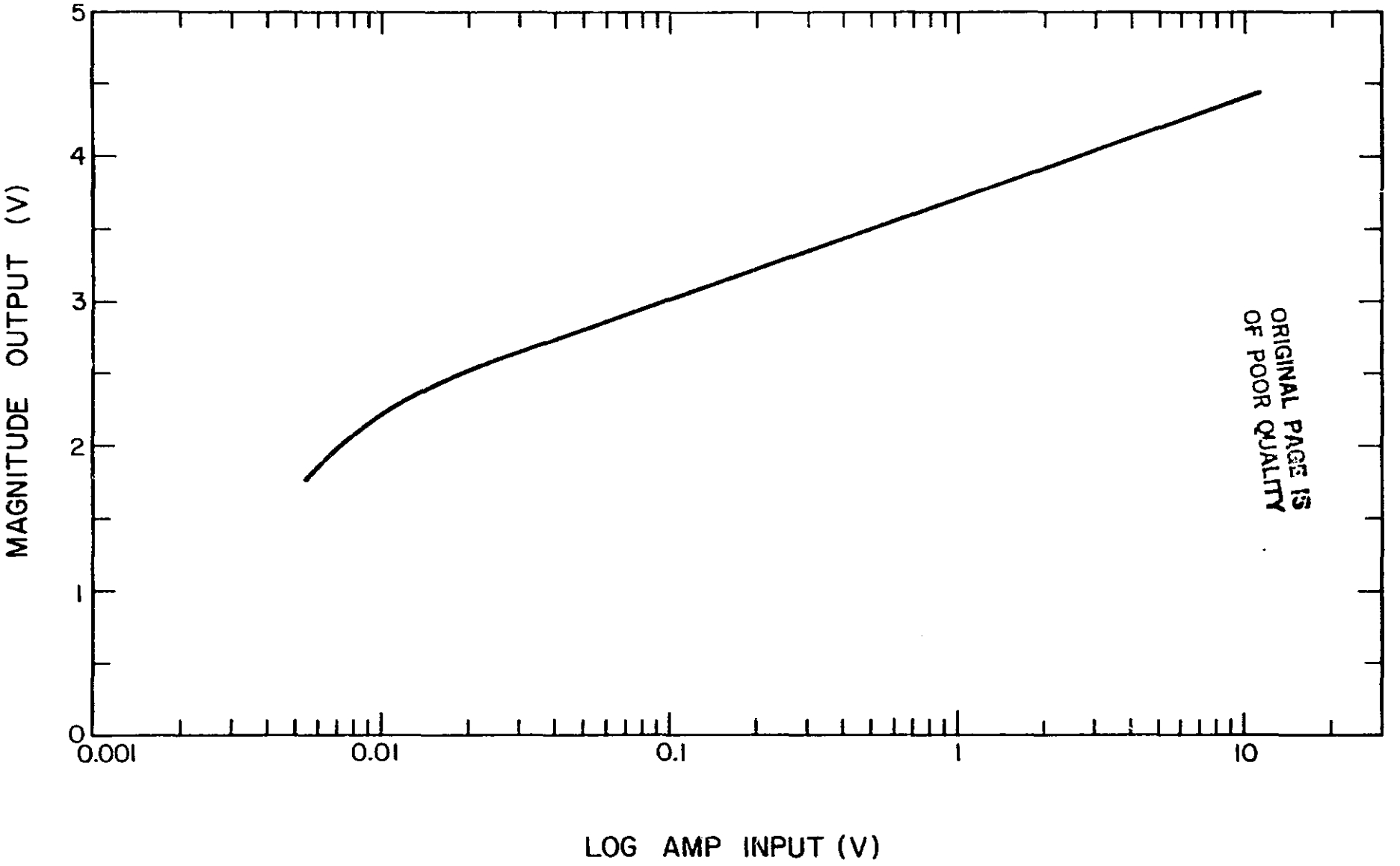

Figure 3.25 Logarithmic amplifier input voltage versus magnitude detector output voltage when operated in temperature regulated cavity (T = 150°F).

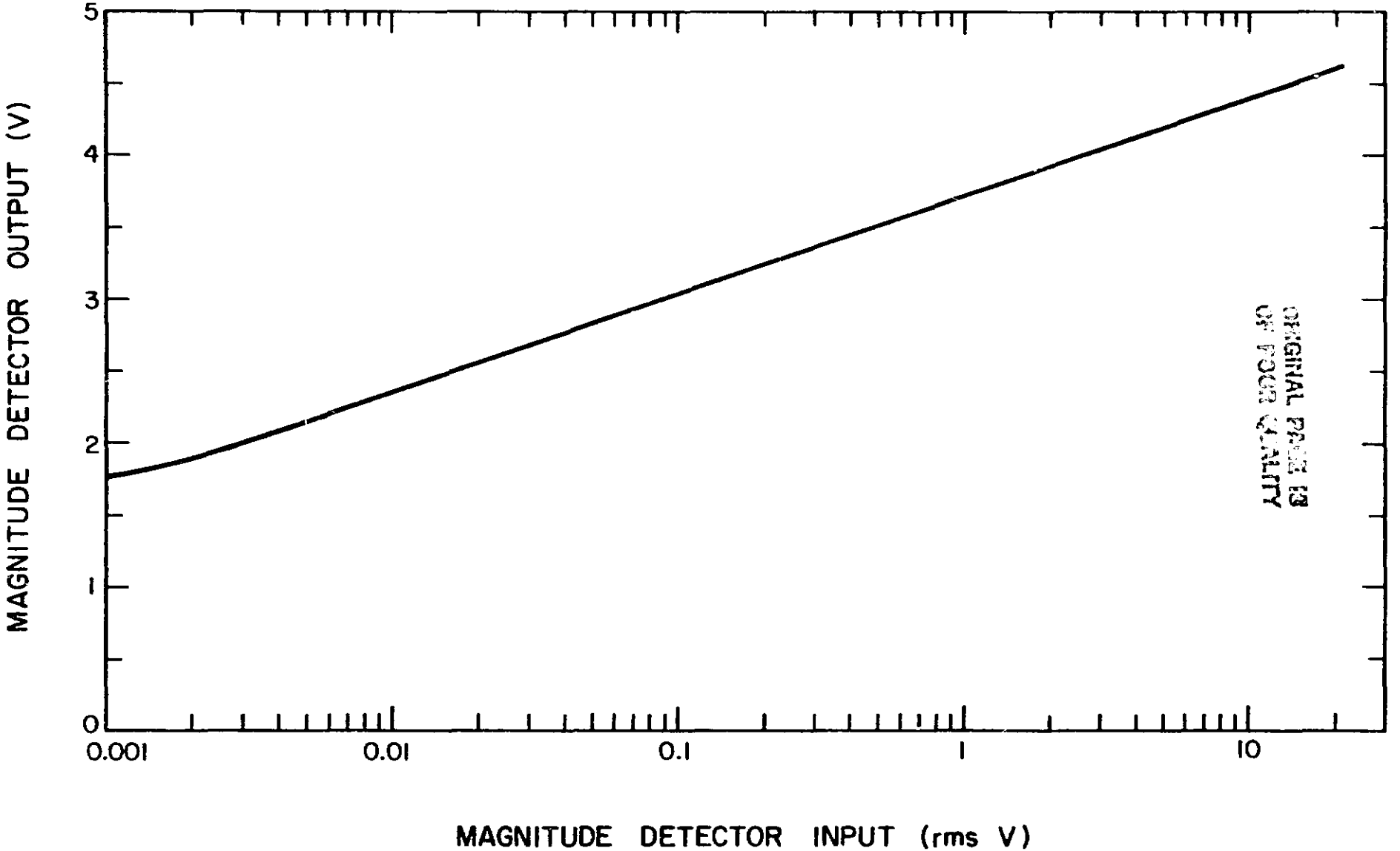

Figure 3.26 Transfer function of the magnitude detector circuit (T = 150°F).

this circuit, Figure 3.9, one is able to measure the hysteresis of the system at test point 7. With the resistor values set as in Figure 3.9, the hysteresis of the systems is ±2 mV; i.e., the input must be greater than +2 mV to switch the output HIGH and less than -2 mV to switch it LOW. If the noise levels of the system warrant more or less hysteresis, R119 should be increased or decreased by the appropriate amount.

The output of the zero crossing detector, which swings from +13.5 V to -13.5 V, is made TTL compatible by the circuits between test points 7 and 8, Figure 3.9. The best way of testing the zero crossing detector is to apply a sinusoid input to the detector and to one channel of a dual trace oscilloscope. The output of the detector, test point 8, should be applied to the second scope channel. By varying the magnitude of the input sinusoid and adding either a dc offset or a noise signal, one is able to check the zero crossing detector. The output of this detector provides the STOP input to the phase detector; the START input is provided by a phase reference signal.

The phase reference START signal is generated by a chopper wheel passing through an optical switch. The output of this switch is made TTL compatible by a Schmidt trigger NAND gate (74132). Figure 3.10 illustrates this circuit and labels its output as test point 9 START. When operating correctly, the START signal should be a square wave with a frequency of four times the frequency of the motor shaft due to the four segments of the chopper blade.

The logic portion of the phase detector circuit, Figure 3.13, has two inputs: test point 8 STOP and test point 9 START. This circuit can be tested using debounced toggle switches at these two test points and observing the output either on an oscilloscope or the LED connected to the output. As previously discussed the circuit sets the output high on the leading edge of the START signal and sets it low on the leading edge of the STOP

signal. Table 3.8 gave the logic expressions for the $\overline{S}$-$\overline{R}$ inputs of the three flip-flops. The circuit built had no problems during testing and performed as expected with both simulated inputs from debounced switches and actual circuit inputs from the optical switch and the zero crossing detector.

3.6.4 *Digital phase display.* The digital phase display, Figure 3.16, has only one adjustment. The 555 must be adjusted so that its frequency is 360 times the frequency of the input sinusoid to the preamplifier. Assuming the input frequency to be 100 Hz the 555 needs to be set to 36 kHz. This enables the unit to display the phase reference output in degrees. R135 is used to adjust the 555 to the desired frequency, Figure 3.16.

4. FLIGHT INSTRUMENTATION

4.1 *Mechanical Design*

The electric field meter is divided into two separate units: the transducer and the signal processing unit. The transducer contains the mechanisms needed to produce a sinusoidal stator area function as well as the electronics that condition the input signal. This signal is further processed by the magnitude and phase detector circuits located in the signal processing unit.

The mechanical arrangement of the transducer is shown in Figure 4.1. There are two internal cavities. One houses the motor whose speed determines the frequency of the input sinusoid. For the four-segment rotor the motor speed is 15 f (rev/min), where the desired operating frequency is f (Hz). Thus to operate at 100 Hz, the motor speed should be 1500 rpm. A Japanese Servo Company DL30S-001 dc motor was selected for its low electrical noise level, high operating speed, and low operating voltage.

The second cavity houses the preamplifier, the optical switch and chopper blade used to generate the reference signal, a coupling between the rotor shaft and the motor shaft, and an assembly to ground the rotor shaft. The preamplifier is placed in a separate cavity in order to shield it from electrical noise. Furthermore, the preamplifier is located as close as possible to the stator to minimize stray capacitance.

Due to the sensitivity of the preamplifier, the coupling between the motor and rotor shafts, and the rotor shaft grounding assembly warrant some discussion. In the preliminary stages of the design, it was thought that a metal coupling of meshing teeth not only provided a means of securely coupling the shafts but it also created a ground path for the rotor. This path had three branches: one through the bearings near the rotor; one through the

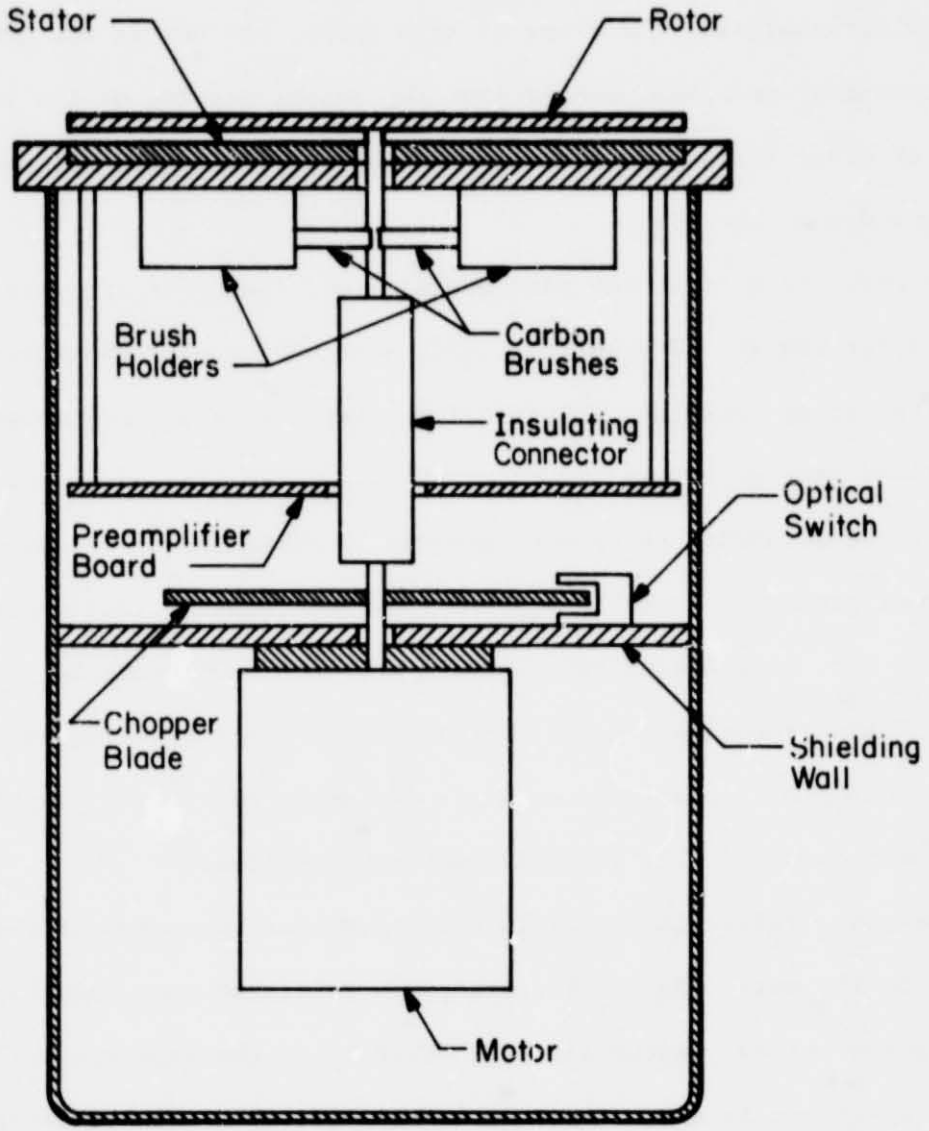

Figure 4.1 Mechanical arrangement of the transducer.

bearings near the motor (via the metal coupler) and one through the motor shaft (which was thought to be at ground potential). Upon testing the unit, it was discovered that the meshing of the coupler teeth produced more noise than was permissible. The cause of this noise, whether it was created by an inconsistent ground path, static from the actual meshing of the coupler teeth, or other sources, was not investigated since it was obvious that the coupler could not be used.

In order to achieve the same goals, i.e., the rotor securely fastened to the motor and a well grounded rotor, a second coupler was tested. Composed of an insulating material cylindrical in shape, this coupler erased the possibility that static on the motor shaft was reaching the rotor. Since two of the three grounding paths were removed by using an insulating coupler, an additional grounding assembly for the rotor was added. This assembly, shown in Figure 4.1, consists of two grounded carbon brushes rubbing on the rotor shaft. These grounding brushes, together with the insulating coupler, provided the best means of achieving a securely fastened, positively grounded rotor. The effectiveness of this assembly has been confirmed.

The phase reference signal is generated by a four-segment chopper blade located on the motor shaft. The signal is generated when the chopper blade disrupts the optical switch which is attached to the aluminum wall separating the two cavities, as can be seen in Figure 4.2, which is the transducer with the cover removed. On the external surface of the transducer head is the stator. The stator, a PC card with the desired area function laid out on it, is countersunk so that it is flush with rim of the transducer. This enables the device to be placed in a payload in a manner which least disturbs

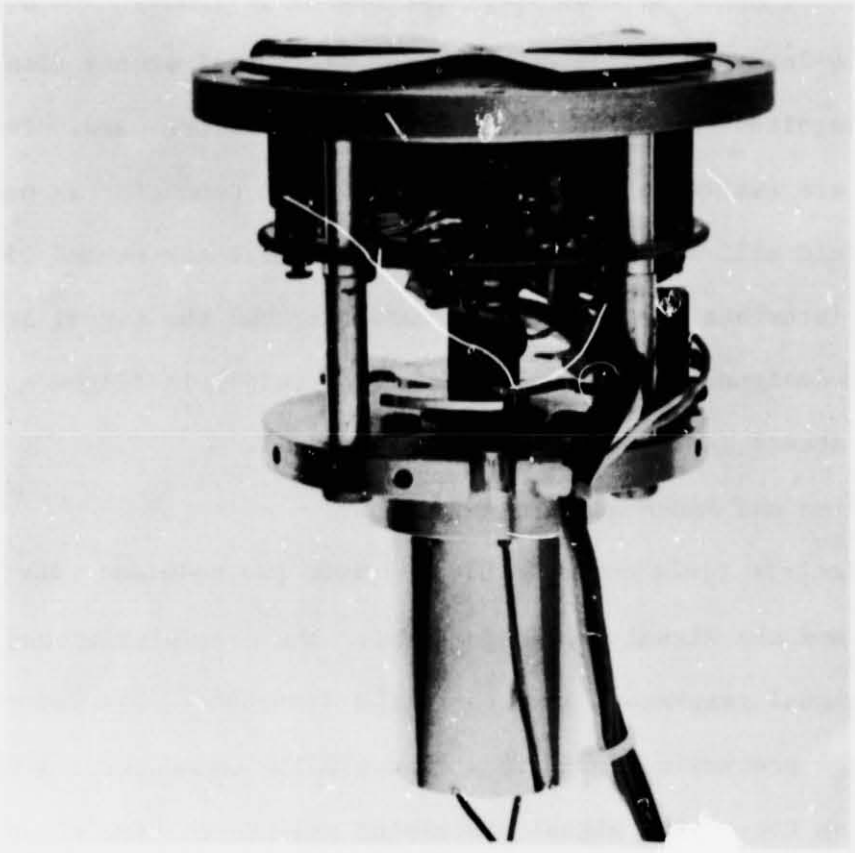

Figure 4.2 Field mill transducer with cover removed.

the electric field. While the electric field transducer is to be flush mounted on the payload with only the surface of the transducer head exposed, the signal processing unit is designed to be internal to the payload.

The signal processing unit, Figure 4.3, is a typical electronic box designed by the Aeronomy Laboratory for use in payloads. The box has room for three 50-lead PC cards although the field mill sensor uses only two cards: a magnitude detector card and a phase detector card. Two external connectors are available on the box. One 15-pin connector is used to interface the field mill sensor with the payload, while the second 15-pin connector is used to interface the field mill transducer and the signal processing unit. The box is designed to hold the PC cards rigidly in flight and also to allow easy access during testing.

4.2 *Packaging and Power Requirements*

The electric field meter is divided into two modules: the transducer and the signal processing unit. The preamplifier and the phase reference signal generator, located in the transducer, are connected to the signal processing unit via a Cannon DA15P connector. A Cannon DA15S is located on top of the signal processing unit to receive these transducer outputs. Table 4.1 lists the pin numbers and their associated signals under the column "Top Connector" for this bus.

These signals are directly connected to a 50-line ribbon cable inside the signal processing unit. This ribbon cable makes it possible for any or all of PC cards to transmit signals to or receive them from the transducer, other PC cards, or the rail in the payload. Table 4.1 lists the pin number of the used ribbon cable lines and their corresponding signals. It should be pointed out that the PC cards in the signal processing unit provide a means of connecting different ribbom cable lines. For example,

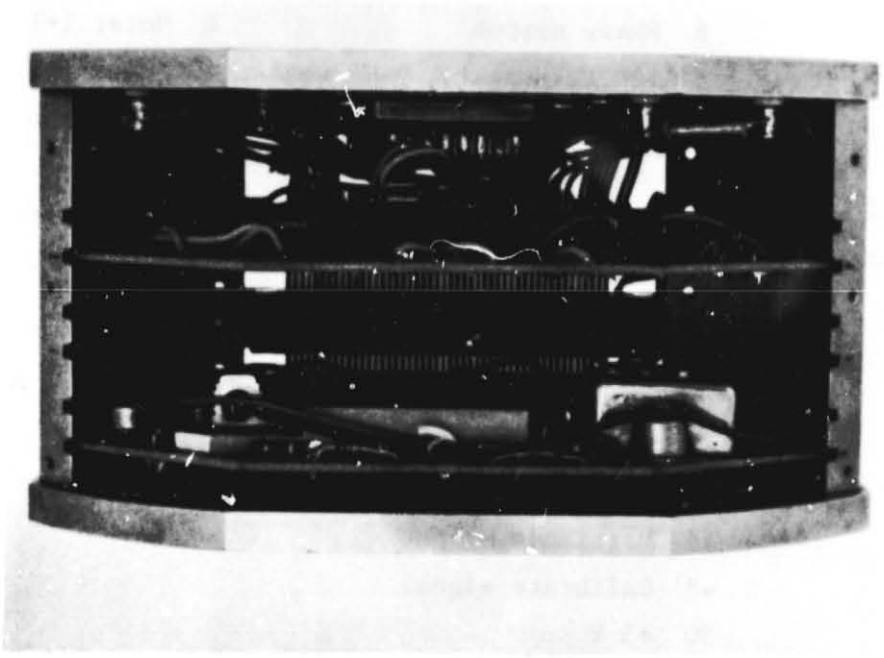

Figure 4.3 Signal processing unit with magnitude detector and phase detector PC cards in place.

Table 4.1 Pin connections for rail connector, ribbon cable and top connector.

RAIL CONNECTOR		RIBBON CABLE		TOP CONNECTOR	
1	-28 V	2	Circuit ground	2	+15 V
2	+28 V	4	+15 V	4	Circuit ground
3	+28 V	6	Phase output	6	Motor (+)
5	Circuit ground	8	+28 V (heater)	8	Preamplifier output
6	Motor and heater ground	30	-15 V	9	Motor ground
9	Calibrate signal	32	+15 V	10	-15 V
10	Magnitude output	34	Circuit ground	11	Phase reference
14	Phase output	36	Motor (+)	12	Co-ax ground
15	+28 V (heater)	38	Preamplifier output		
		40	Motor and heater ground		
		42	Phase reference		
		44	Circuit ground		
		46	Magnitude output		
		48	Calibrate signal		
		50	+5 V		

line #4 of the ribbon cable is the true +15 V line but a jumper on the magnitude detector PC card makes line #32 of the ribbon cable +15 V also. Therefore, Table 4.1 describes the situation only when the magnitude or phase detector printed circuit card is in place.

The transducer is connected to the payload by a second Cannon DA15P connector located on the back of the signal processing unit. This connector interfaces with the rail (wiring conduit) in the payload which requires that the rail connector pins (Table 4.1) be labeled in accordance with the existing payload lines. Table 4.2 lists the direct interconnection of the three signal buses with each other. These three buses (from the transducer to the signal processing unit, inside the processing unit, and from the signal processing unit to the rail) all have unused lines which makes future improvements easy to accommodate.

There are four operating voltages in the electric field meter: +28 V, +15 V, -15 V, and +5 V. These voltages are used to power the logarithmic amplifier's heating resistor (+28 V), the operational amplifiers (±15 V), and the TTL circuit (+5 V). In addition, a separate voltage source is needed to run the motor. Table 4.3 lists the supply voltages and the current drawn from each.

In order to reduce the number of supply lines required by the circuit, only +28 V, -28 V, power ground, and signal ground are used to connect the electric field meter. These four lines, which are available on the rail connector, are subsequently used to derive the necessary supply voltages using National Semiconductor 78XX and 79XX voltage regulators. These regulators, which are attached to the walls of the signal processing unit, are capable of supplying 1 A each. Referring to Table 4.3, it is evident that no

Table 4.2 Direct interconnections between rail connector, ribbon cable and top connector.

SIGNAL	RAIL CONNECTOR	RIBBON CABLE	TOP CONNECTOR
Circuit	Pin 5	Pins 34, 44, 2	Pins 4, 12
Motor and heater ground	Pin 6	Pin 40	Pin 9
Calibrate	Pin 9	Pin 48	
Magnitude output	Pin 10	Pin 46	
Phase output	Pin 14	Pin 6	
+28 V (heater)	Pin 15	Pin 8	
+15 V		Pin 32	Pin 2
Motor (+)		Pin 36	Pin 6
Preamplifier output		Pin 38	Pin 8
-15 V		Pin 30	Pin 10
Phase reference		Pin 42	Pin 11

Table 4.3 Power requirements from individually regulated sources.

REGULATOR VOLTAGE	HEATER ON		HEATER OFF	
	CURRENT (mA)	POWER (W)	CURRENT (mA)	POWER (W)
+28 V (heater)	280	7.84	0	0.0
+15 V	390	5.85	390	5.85
-15 V	26	0.39	26	0.39
+5 V	78	0.39	78	0.39
+5.5 V (motor)	290	1.60	290	1.60

Table 4.4 Payload power requirements.

SUPPLY VOLTAGE	HEATER ON		HEATER OFF	
	CURRENT (mA)	POWER (W)	CURRENT (mA)	POWER (W)
+28 V	755	21.14	480	13.44
-28 V	30	0.84	30	0.84

regulator is being overloaded as all the supply currents are under 1 A. Table 4.4 lists the power requirements of the +28 V and -28 V supply lines from the rail.

As previously mentioned, the system used two grounds; a power ground and a circuit ground. The circuit ground, as the name implies, is used for all the electronic circuits while the power ground is used by the dc motor and the logarithmic amplifier heating resistor. Use of two grounds reduces noise in the system and prevents any single ground wire from carrying excessive currents.

4.3 *Flight Configuration*

In order to measure the atmosphere's electric field, two or more electric field meters will be needed. This is due to the possible charge on the rocket causing its potential to be different from ambient. One practical configuration for the placement or two independent electric field meters is illustrated in Figure 4.4. Electric field meter #1 is located at the front of the rocket, on the nose cone, while electric field meter #2 is placed on the cylindrical section. Since the rocket is spinning in flight, this second electric field meter can be modeled as two diametrically opposed units.

With the information provided by the two field meters, one can calculate the (vector) ambient electric field and the charge on the rocket. However, due to the irregular shape of the rocket, this calculation is difficult. An estimate of the effect of the shape can be accomplished by modelling the rocket and payload as an ellipsoid. In this model, with the electric field meters positioned on the major and minor axes, one can make use of existing solutions for the purely electrostatic case. Exact solutions are also possible which account for finite conductivity.

A second approach is to build a mock-up payload (in lightweight metal or metal-covered plastic) and calibrate the system in the lower

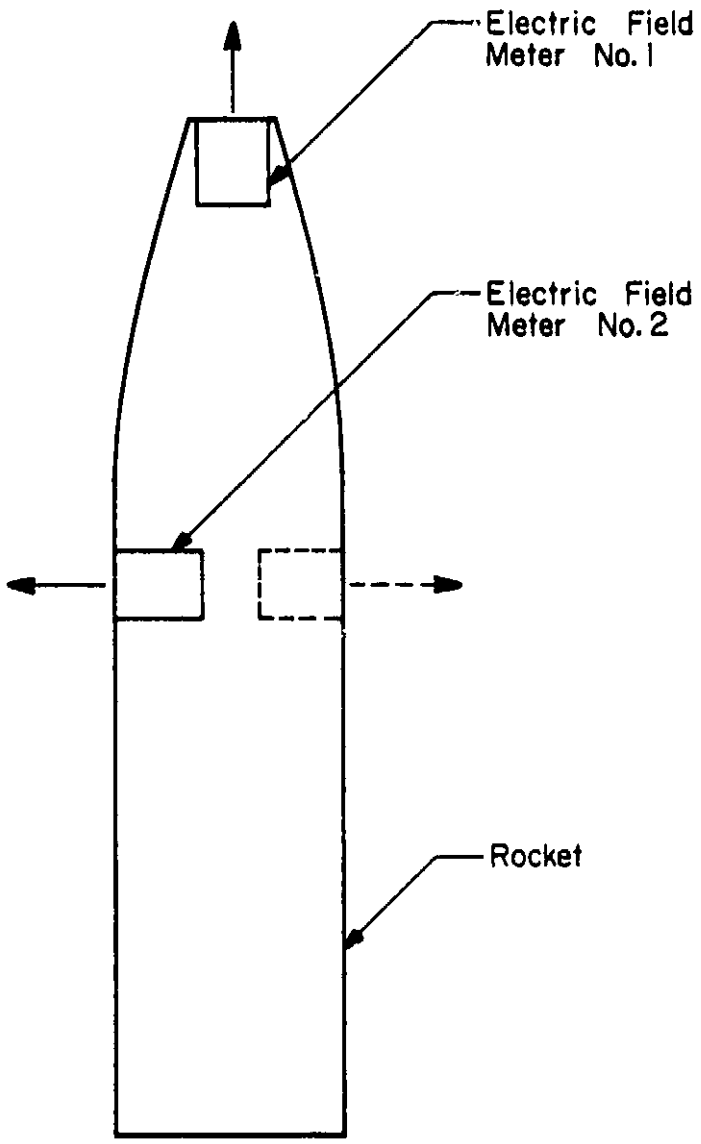

Figure 4.4 Suggested flight configuration using two electric field meters to measure the atmospheric electric field and conductivity.

atmosphere. This approach should prove to be more acceptable since the actual shape of the rocket is taken into account. Once this calibration is completed, one can model the payload as an ellipsoid to get a check on the accuracy of the first approach by comparing the results. In either case, a scale model would be needed.

5. TEST AND SIMULATION

5.1 *Electric Field Meter*

5.1.1 *Introduction.* The instrument can be tested for response to electric fields by applying such a field to the exposed surface of the transducer. This is accomplished using a parallel-plate arrangement with a hole cut in one plate to accommodate the transducer, as shown in Figure 5.1. A known voltage, V, is applied between the plates. With a separation distance, d, between the plates the electric field at the stator, neglecting a correction due to edge effects, is given by

$$E = V/d \tag{5.1}$$

In the system shown in Figure 5.1, the separation is 25.4 mm.

5.1.2 *Preamplifier noise.* Initial tests of the field meter using the parallel-plate arrangement revealed an important, but unwanted, component of the signal at the input. The output of the preamplifier is, as expected, a sinusoidal signal at 100 Hz, with no dc offset. When first turned on and with no applied field (i.e., V = 0 in equation (5.1)) the peak voltage at the preamplifier output was 465 mV, corresponding to 85 pA at the input. This noise level existed when the stator was connected to the preamplifier. With the stator disconnected the unwanted signal was reduced to 5.5 mV at the output, (1 pA at the input).

It was also found that the unwanted signal (with the stator reconnected to the input) could be reduced below that of the unconnected preamplifier by applying a voltage -0.38 V to the parallel-plate test fixture. This last test showed that the unwanted signal is a displacement current.

The origin of the unwanted signal is the varying capacitance between rotor and stator when there is a voltage between the two. There are two

Figure 5.1 The transducer of the electric field meter on the parallel-plate test fixture.

principal sources of this voltage. One is the input offset voltage of the first operational amplifier. This is already small in the AD515J (3 mV, maximum; 0.4 mV, cypical) and can be nulled by external adjustment. The input offset voltage drift is 50 μV/°C so that some residual effect must be anticipated. It can be noted that the AD515K has superior specifications for input offset voltage: 1 mV maximum, 0.4 mV typical with 15 μV/°C drift.

There is a second source for the voltage between rotor and stator.. It is the difference in work function of the two adjacent surfaces. If the work function of each was constant over the surface then the input offset voltage of the operational amplifier (AD515J) could be adjusted to give zero signal at the input of the preamplifier. The limiting factor is the uniformity of work function over the surface since the movement of one plate over the other exposes different areas of surface.

The magnitude of the displacement current caused by the varying capacitance can be estimated. The capacitance of the rotor-stator assembly has a maximum value (when the stator is fully covered)

$$C_m = 2\varepsilon_o A_o / D \tag{5.2}$$

where $2A_o$ is the total area of the stator (13.3 cm^2) and D is the distance between rotor and stator. This distance is not precisely defined (or even precisely constant) in the present instrument but a value of .7 mm is typical. The value of C_m is thus about 6 pF.

Since the capacitance is proportional to the area covered

$$C = (C_m/2)(1 + \cos\omega t) \tag{5.3}$$

With a fixed voltage difference V_c between rotor and stator the displacement current due to varying capacitance is

$$i_{dc} = V_c \frac{dC}{dt} = -V_c (C_m/2)\omega \sin\omega t \tag{5.4}$$

which has a peak value

$$i_{dcm} = V_c C_m \omega/2 \tag{5.5}$$

For an operating frequency of 100 Hz the peak displacement current is

$$i_{dcm} = 2 \times 10^{-9} V_c \tag{5.6}$$

Thus a potential difference of 1 mV gives rise to a displacement current of 2 pA at the input to the preamplifier.

The varying capacitance is the practical factor limiting the sensitivity of the electric field meter. Using the input offset voltage null adjustment of the first operational amplifier allows the unwanted signal to be reduced to 4 pA. Further reduction, if desired, could be accomplished by increasing the separation of rotor and stator (C_m would decrease) and by carefully treating the surfaces of rotor and stator by, for example, plating with gold or by coating with Aquadag (colloidal graphite). Also the temperature dependence would be reduced by substituting the AD515K for the AD515J as the first operational amplifier.

The present system is capable of detecting the anomalous electric fields of the middle atmosphere (>0.1 V/m). However, if it is desired to improve the sensitivity of the electric field meter the unwanted signal at the input of the preamplifier will be the major problem to be addressed.

5.1.3 *System adjustment.* With the field mill transducer connected to the signal processing unit, it is possible to test the entire system. First, the motor speed should be 1500 rpm which corresponds to an input frequency of 100 Hz. This can be checked by monitoring the phase reference signal, test point 9 Figure 3.10, on an oscilloscope or frequency counter. Alternately, one could monitor the output of the zero crossing detector, test point 8 Figure 3.9.

The position of the chopper blade on the rotor shaft is important since it is the means by which the phase angle is derived. The easiest method of positioning the chopper blade is to monitor both the phase detectors START signal and STOP signal; test points 8 and 9 Figures 3.10 and 3.9. A 0° phase angle corresponds to when the leading edges of the pulses found at these test points occur concurrently. If the unit is operated on the ground (or in a laboratory) where the conduction current is negligible, the chopper blade should be positioned such that the phase angle is zero when operated in a positive electric field as the input current would essentially be all displacement current. If a dual trace oscilloscope is not available, one may use a single trace oscilloscope and monitor the phase output signal. This signal should be constantly LOW, corresponding to 0° or constantly HIGH, corresponding to 360°.

Once the chopper blade is correctly positioned, the digital phase display board can be calibrated. With its input connected to the phase detector output, R135 of Figure 3.16 should be adjusted so that the display reads 0°.

One may check the operation of the phase detector by introducing a conduction current at the input. If the conductivity between the parallel test plates is increased, the phase angle displayed on the digital phase display board should read between 0° and 90° for positive electric fields and between 180° and 270° for negative electric fields. The conductivity could be increased by using a radioactive source to ionize the air between the plates. In this case, both conduction currents and displacement currents will be present at the preamplifier input.

Once the phase detector has been tested and calibrated, the magnitude detector should be examined. To begin with, the temperature regulated cavity

should be brought up to operating temperature, 150°F, approximately five minutes. To be sure the cavity is up to its operating temperature, the voltage at the output of operational amplifier A16, Figure 3.5, should be measured. If the voltage is +15 V, the heater is still on. A voltage of -15 V means the cavity has reached its operating temperature. At this point, a calibrate signal of +5.0 V should be applied to the input of the logarithmic amplifier, Figure 3.4. The actual operating temperature of the device can be found from Figure 3.22 by noting the resulting magnitude output and finding the appropriate temperature curve. This curve should be the single curve shown in Figure 3.25.

After the logarithmic amplifier's temperature has been verified to be 150°F, one can use Figure 3.26 as the transfer function of the magnitude detector circuit. This graph was obtained by placing sinusoid inputs into the magnitude detector (operating at 150°F) and measuring the resulting output voltage.

The next step is to get a transfer function for the preamplifier - neglecting the phase of the input. If the stator is disconnected and a sine wave is fed to the input of the preamplifier through a capacitor, one obtains a known input current to the preamplifier

$$i_{in} = C\frac{dV}{dt} \tag{5.7}$$

with

$$V = V_o \sin\omega t \tag{5.8}$$

gives

$$i_{in} = CV_o\ \omega\ \cos\omega t \tag{5.9}$$

With an input capacitor of 10 pF and an operating frequency of 100 Hz this gives

$$i_{in} = 6.3 \times 10^{-9}\ V_o\ \cos\omega t \tag{5.10}$$

Using known input voltages, and therefore known input currents, one is able to derive an expression relating the input current (pA RMS) to the preamplifier output (V RMS); Figure 3.20. This expression combined with the magnitude detector's transfer function yields a plot of input current (100 Hz sinusoid, pA RMS) versus magnitude output (volts dc); Figure 5.2.

Reconnecting the stator to the preamplifier, one can use Figure 5.2 to determine the input current induced by an electric field by knowing the output voltage of the magnitude detector circuit. Once the input current and the phase angle, ϕ, are known, equations (2.14) and (2.15) can be used to determine the atmosphere's conductivity and electric field.

5.2 *Payload System*

This section deals with the basic tests needed to confirm proper operation of the electric field meter installed in the payload.

The unit should be placed on external power for at least ten minutes to allow the temperature-regulated cavity time to reach its operating temperature. While still on external power, the calibrate signal should be applied. With an input of +5.0 V to the logarithmic amplifier, Figure 3.22 can be used as a check on the operating temperature by noting the magnitude of the output voltage. If the unit is operating at the desired 150°F, this output voltage should also fall on the curve in Figure 3.25. After the operating temperature has been verified, the next task is to check the operating frequency.

If further tests are desired one can apply a test input to the preamplifier. Recalling that the stator is connected directly to the preamplifier input, a current input can be injected to the preamplifier as discussed in section 3.5. Clamping one lead of a capacitor to the stator, a voltage applied across the other lead and ground produces an input current predicted by equation (5.4).

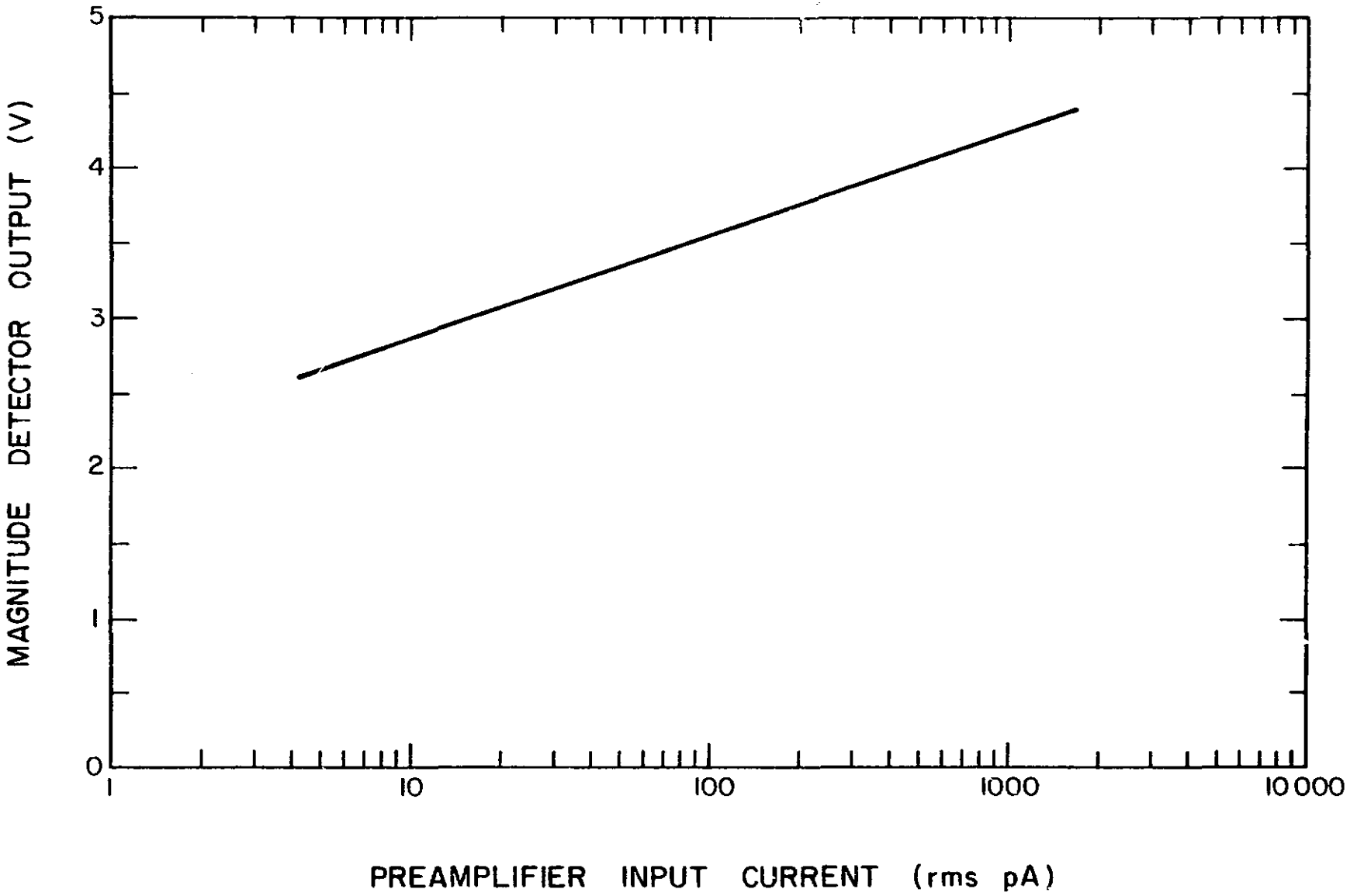

Figure 5.2 Transfer function of electric field meter's magnitude detector circuit: input current to the preamplifier versus magnitude detector output voltage.

Under this test condition, the rotor should be stopped so that the operator knows that the input current is comprised only of the current passing through the capacitor and not conduction or displacement currents induced by the rotor-stator pair. Knowing the input current in pA RMS and measuring the corresponding magnitude output voltage, the operator can get a check on the validity of the data in Figure 5.2.

For launch, the unit should be placed on internal power and the heater supply voltage turned off (pin 15 from the payload rail). This step reduces the current drawn by the electric field meter by 275 mA (refer to Table 4.4). The foam encapsulation of the instrumentation will keep the temperature of the cavity constant (at 150°F) for the duration of the flight (less than ten minutes). To check this, the calibrate signal should be applied just before take-off and shortly before landing to verify the cavity temperature.

Finally, since this unit is a prototype electric field meter, further insight into its performance would be desirable during the first flight test. To this end, it is recommended that the output of the preamplifier (test point 2, Figure 3.2) and the phase reference signal (test point 9, Figure 3.10) be transmitted in addition to the magnitude detector output and the phase detector output.

6. SUGGESTIONS FOR FUTURE WORK

The design, construction, and testing of the prototype electric field meter have been carried out in conjunction with constant evaluation of the system. Although the unit operates with adequate sensitivity it is believed that the system can be improved with respect to sensitivity and in other ways.

The dc motor (DL30S) used to drive the rotor could be replaced by the DL40S; a motor made by the same company but one which offers more torque. Also, the DL40S operates from 24 V, compared to the 12 V needed by the DL30S; thus the current drain from the payload batteries would be reduced.

A hybrid phase-locked loop (PPL) system could also be implemented to insure the proper rotor speed. The phase reference pulse, available at test point 9, Figure 3.10, could be used as one input to the PPL, with an independently generated 100 Hz signal acting as a reference. The automatic gain control of the PPL could then be used to adjust the motor supply voltage to obtain the desired speed, as indicated in Figure 6.1.

An alternative to the dc motor with a phase-locked loop feedback system is to use a stepping motor. The motor could then be driven at the desired speed by a sequence of digital pulses derived from a fixed frequency source. With a rotor speed of 1500 rpm, the choppy motion of the motor should be insignificant.

The bearings used to position the rotor shaft proved to be a source of noise. For this reason, further investigation into the selection of bearings is warranted. Also, since the bearings do not provide a definite ground path for the rotor, one might explore the possibility of insulating the bearings from the rest of the unit thus relying on the brushes for grounding.

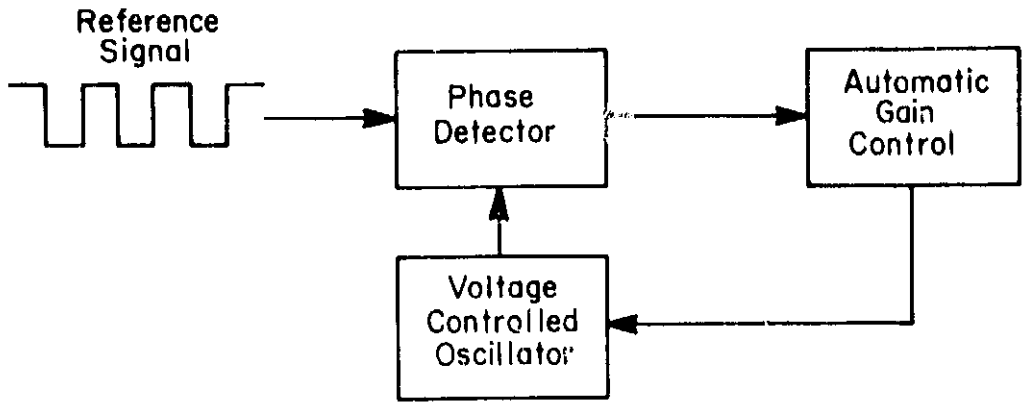

(a)

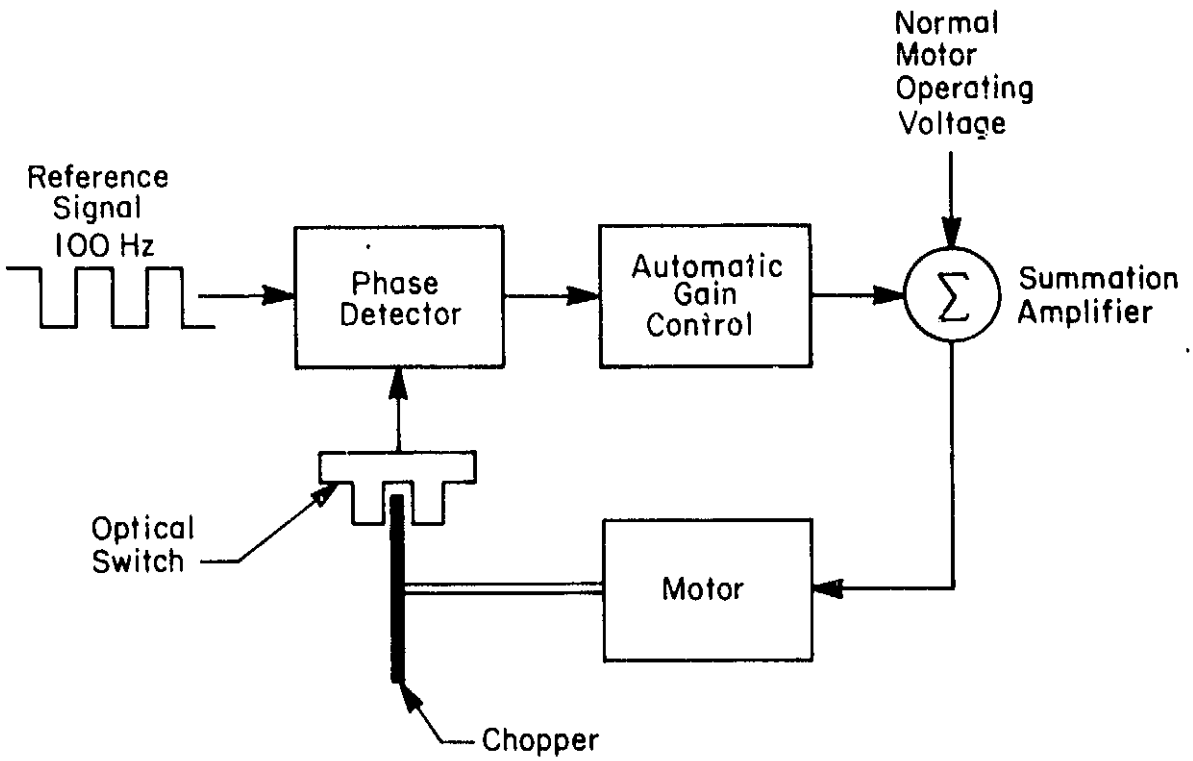

(b)

Figure 6.1 (a) Block diagram of a typical phase-locked loop system. (b) Block schematic of a hybrid phase-locked loop system which could be used to regulate the motor speed. The combination of the motor, chopper blade, and the optical switch replaces the voltage controlled oscillator.

Another useful modification would be to implement an electronic method of adjusting the phase reference signal. Although one can adjust this signal by repositioning the chopper blade on the motor shaft, an electronic adjustment would be quicker and simpler. One proposed method is to use an R-C network at test point 9 in Figure 3.10. The voltage at test point 9, rising exponentially, is compared with a reference voltage by a simple comparator, as shown in Figure 6.2. The R138 - C116 pair should be chosen such that the rise time is approximately 5 ms for the operating frequency of 100 Hz. In addition, the R-C pair must be compatible with the output source current and output sink current of the 74132. The diode in parallel with the resistor R138 is a means by which capacitor C116 can be discharged between cycles. By changing the reference voltage at the inverting input of the comparator, one essentially selects a different point on the exponential voltage curve at the non-inver input, thus changing the time the phase reference signal occurs, test point 9.

Another mechanical improvement would be to extend the transducer head further into the protective metal case. Then, additional screws could be used to hold the transducer head to the case; refer to Figure 4.2. Presently, the transducer and plate are held in place by standoffs extending from the cavity separation wall which, in turn, is held to the case by eight screws, seen in Figure 4.1. The additional screws would not only reduce vibrations and add support, but also, they would make a more positive ground for the transducer head.

Shifting the attention to the rotor and stator, it has been found that the present combination produces a slight dc offset voltage at the input to the preamplifier. This offset is attributed to a difference in work function between the stainless-steel rotor and the tin-plated stator. An obvious

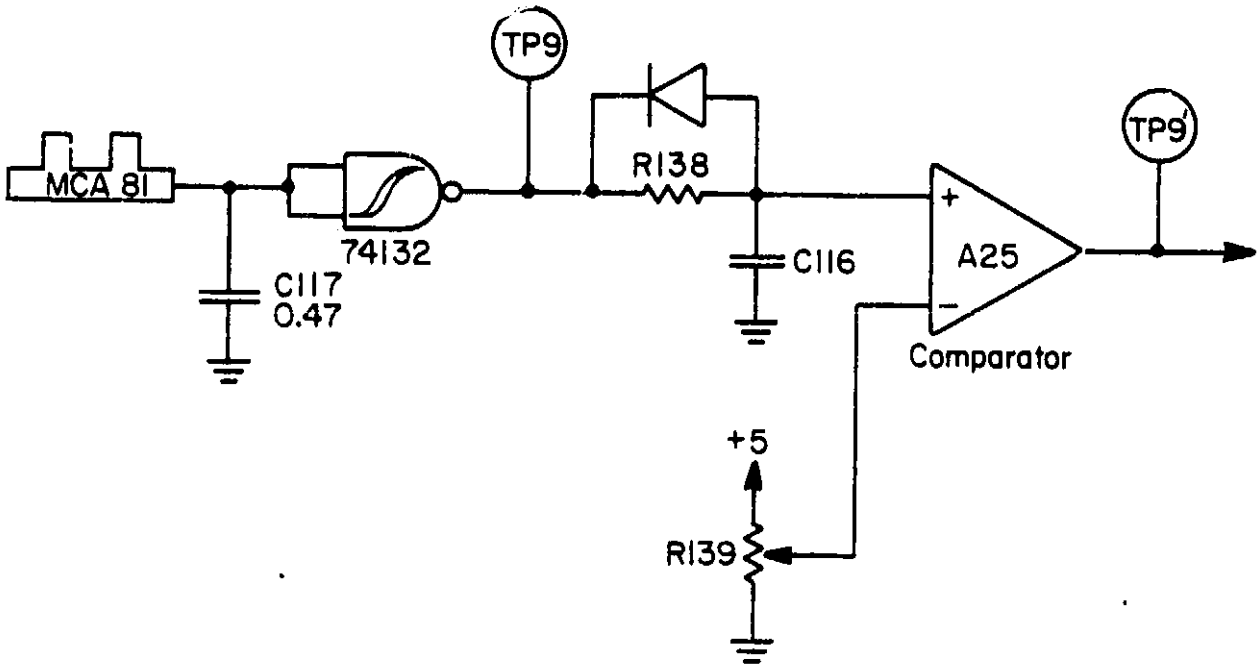

Figure 6.2 Block schematic of an electronic phase adjustment circuit. Input phase reference signal (test point 9) can be delayed before reaching test point 9 by an amount determined by resistor R139.

solution is to gold plate the rotor and stator, thus largely removing the work function difference in addition to protecting the surfaces from oxidation.

Equations (2.4) and (2.5) predict that the magnitude of the conduction current and the displacement current are linearly dependent on the area of the stator. Therefore, in order to achieve greater sensitivity and obtain stronger input signals, the area of the stator should be as large as permissible. This is, however, a consideration involving the size of payload in which the instrument will be flown.

The preamplifier of the electric field meter might be improved by slight revisions in the picoampere-to-voltage converter: the AD515J in Figure 3.2. An applications note for the AD515J offers several suggestions. First, the operational amplifier should be as close as possible to the signal source. In addition, the PC board should be laid out in a manner which makes use of the AD515J's guard pin, pin #8. Analog Devices also recommends that the device be placed in a teflon IC socket in order to reduce leakage currents. Finally, the device should be well cleaned and operated in an environment of low humidity.

If the AD515J proves to be too insensitive for small signals, the unit could be replaced by the Analog Device model 310J: an ultra-low-bias-current varactor-bridge operational amplifier. Having a guaranteed input bias current of 10^{-14} amps or less, this modular unit can be connected in the same configuration as the AD515J. However, it should be pointed out that the present system has noise levels which render the added sensitivity of the AD310J useless. Therefore, it is essential that the noise in the present system be reduced before one can justify the alternative of the AD310J.

One method of reducing the noise inherent to the system is to replace the rotor bearings, as has been mentioned. Another method is to install a bandpass filter following the preamplifier. At the start of the project, a National Semiconductor LF100-C was used as such a filter. This single IC chip, which can be connected to function as numerous filters, was connected as a bandpass filter with a center frequency of 100 Hz and a Q of 2. This would block the high frequency noise as well as block any dc signals on the preamplifier output. Upon further investigation, the LF100-C proved to be inadequate for two reasons. First, the phase shift of the device was not uniform over the range of expected input voltages. Second, the device did not function at signal levels in the vicinity of 2 mV, a voltage which was expected to be encountered in normal circuit operation. Therefore, the bandpass filter was omitted from the circuit. An alternate approach to the problem would be to design a bandpass filter using a high-pass filter followed by a low-pass filter. The two filters, acting as a bandpass filter, could be made from operational amplifiers that would function over the desired signal range of 2 mV to 18 V.

One final suggestion deals with the gain amplifier following the logarithmic amplifier, Figure 3.4. As shown in Figure 3.24, the output of the logarithmic amplifier has the range -500 mV to -200 mV. By placing a constant voltage of -200 mV on the non-inverting input of the gain amplifier, the LM201, the output of the logarithmic amplifier could essentially be viewed as having a range from -300 mV to zero. In this case, the gain of the LM201 could be increased from 10 to 16, giving the system a somewhat better resolution on the magnitude of the input signal. Presently, the magnitude output falls in the range 2 V to 5 V. If the offset is applied to

the gain amp, the magnitude output uses the full range (0 to 5 V) of the telemetry system.

REFERENCES

Bragin, Y. A., A. A. Tyutin, A. A. Kocheev and A. A. Tyutin [1974], Direct measurement of the atmosphere's vertical electric field intensity up to 80 km, *Cosmic Res.*, *84*, 279-282.

Cole, R. K. and E. T. Pierce [1965], Electrification in the Earth's atmosphere for altitudes between 0 and 100 kilometers, *J. Geophys. Res.*, *70*, 2735-2749.

Gish, O. H. and G. R. Wait [1950], Thunderstorms and the Earth's general electricification, *J. Geophys. Res.*, *55*, 473-484.

Hale, L. C. and C. L. Crosky [1979], An auroral effect on the fair weather electric field, *Nature*, *278*, 239-241.

Hale, L. C., C. L. Crosky and J. D. Mitchell [1981], Measurement of middle-atmosphere electric fields and associated electrical conductivities, *Geophys. Res. Lett.*, *8*, 927-930.

Hays, P. B. and R. G. Roble [1979], A quasi-static model of global atmospheric electricity. 1. The lower atmosphere, *J. Geophys. Res.*, *84*, 3291-3305.

Kelley, M. C., R. F. Pfaff, C. Siefring and R. Green [1982], On the reality of volt/meter middle atmospheric electric fields, *EOS Trans.*, *63*, 337.

Mauchly, S. J. [1923], Diurnal variation of the potential gradient of atmospheric electricity, *Terr. Magn. Atmos. Elect.*, *28*, 61-81.

Maynard, N. C., C. L. Crosky, J. D. Mitchell and L. C. Hale [1981], Observations of volt/meter vertical electric fields in the middle atmosphere, *Geophys. Res. Lett.*, *8*, 923-926.

Maynard, N. C., F. J. Schmidlin, L. C. Hale and C. L. Crosky [1982], Middle atmosphere campaign: Electric field structure in the high latitude middle atmosphere, *EOS Trans.*, *63*, 337.

Mozer, F. S. [1971], Balloon measurements of vertical and horizontal atmospheric electric fields, *Pure Appl. Geophys.*, *84*, 32-45.

Muroga, S. [1979], *Logic Design and Switching Theory*, John Wiley and Sons, New York.

Pfaff, R., M. C. Kelley, P. Kintner, C. Cornish, R. Holzworth and L. Hale [1980], Simultaneous measurements of mesospheric and stratospheric electric fields on two rockets and a balloon, *EOS Trans.*, *61*, 1056.

Reid, G. C. [1979], The middle atmosphere. In *Middle Atmosphere Electrodynamics*, edited by N. C. Maynard. NASA CP-2090, 27-42.

Roble, R. G. and P. B. Hays [1979], A quasi-static model of global atmospheric electricity. 2. Electrical coupling between the upper and lower atmosphere, *J. Geophys. Res.*, *84*, 7247-7256.

Tyutin, A. A. [1976], Mesospheric maximum of the electric-field strength, *Cosmic Res.*, *14*, 132-133.

Whipple, F. J. W. and F. J. Scrase [1936], Point discharge in the electric field of the Earth, *Geophys. Mem., Lond.*, *68*, 1-20.

Wilson, C. T. R. [1920], Investigations on lightning discharges and on the electric field of thunderstorms, *Phil. Trans. A.*, *221*, 73-115.